STIMULATION AND RESERVOIR ENGINEERING OF GEOTHERMAL RESOURCXS

Henry J. Ramey, Jr., and A. Louis London
Co-Principal Investigators
Stanford University
Stanford, California

Progress Report No. 4

August, 1975

Grant No. AER72-03490-A.03
(Previous Grant No.GI-34925)

to

Division of Advanced Energy Research and Technology
National Science Foundation
Washington, D. C.

TABLE OF CONTENTS

Page

LIST OF FIGURES

LIST OF TABLES

INTRODUCTION

The Stanford University research program on the study of stimulation and reservoir engineering of geothermal resources started in September, 1972, as an interdisciplinary program. The broad objectives of this program include:

(1) the development of experimental data and computational procedures to evaluate the optimum performance of fracture-stimulated geothermal reservoirs;

(2) the development of physical and mathematical geothermal reservoir models to evaluate important thermophysical, hydrodynamic, and chemical parameters based on fluid-energy-volume balances as part of reservoir engineering practice; and

(3) the construction of a laboratory model of an explosion-produced chimney to obtain experimental data on the processes of in-place boiling, moving flash fronts, and two-phase flow in porous and fractured hydrothermal reservoirs.

The project was initiated as a joint program between the Civil Engineering Department of the School of Engineering and the Petroleum Engineering Department of the School of Earth Sciences. Starting during the second year of the program, assistance was provided by the Mechanical Engineering Department of the School of Engineering, and during the current year, by the Department of Geology, School of Earth Sciences. Personnel who have contributed to the preparation of this progress report are:

Prof. Henry J. Ramey, Jr., Petroleum Engr. Dept., Co-Principal Investigator

Prof. A. Louis London, Mechanical Engr. Dept., Co-Principal Investigator

Prof. William E. Brigham, Petroleum Engr. Dept., Faculty Associate

Prof. James 0. Leckie, Civil Engr. Dept., Faculty Associate

Dr. Norio Arihara, Petroleum Engr. Dept., Postdoctoral Fellow

Mr. Paul Atkinson, Petroleum Engr. Dept., Research Assistant

Mr. Francis J. Casse, Petroleum Engr. Dept., Research Assistant

Mr. Hsiu-Kuo Chen, Petroleum Engr. Dept., Research Assistant

Mr. Stephen D. Chicoine, Petroleum Engr. Dept., Research Assistant

Mr. Roger P. Denlinger, Geophysics Dept., Research Assistant

Mr. Anstein Hunsbedt, Civil Engr. Dept., Research Assistant

Mr. James A. Liburdy, Civil Engr. Dept., Research Assistant

Mr. M. C. Tom Kuo, Civil Engr. Dept., Research Assistant

Mr. Alan K. Stoker, Civil Engr. Dept., Research Assistant

Mr. Alvaro Umana, Civil Engr. Dept., Research Assistant

In addition to the preceding personnel, Mr. Jon Grim joined the staff during the year as a Technician-Research Assistant. He has made many valuable contributions to the experimental phases of the program. Finally, Prof. Paul Kruger took leave from the University in June, 1974 to join the National Science Foundation RANN geothermal staff. Prof. London replaced him as Co-Principal Investigator for the current period. Prof. Frank W. Dickson, Associate Chairman, Geology Department, directed chimney model monitoring, and Prof. George A. Parks, Dept. of Applied Earth Sciences, assisted in other areas.

Rapid developments occurred in all projects in the program during the current annual period. A project review presentation was held during May, 1975, in conjunction with the 2nd United Nations Geothermal Symposium in San Francisco. The project review included participants from industry, university, and government agencies in keeping with the objectives of the RANN Program of the National Science Foundation. Many of the results given in this report were described at the Project Review Presentation.

Because of rapid developments in mature projects, a number of publications were released this year. Six Stanford Geothermal Program Technical Reports were issued (SGP-TR-2 through 7) and widely distributed; three program papers were presented at the United Nations Geothermal Symposium; one program paper was presented at the California Regional Meeting of the Society of Petroleum

Engineers in April, 1975, and accepted for publication; and two additional papers on transient pressure analysis for geothermal wells were presented at the UN Geothermal Symposium by Stanford Geothermal Program personnel. References for all Program Reports and publications are given in this report.

Although pressure transient analysis has not been a part of the Program, several of the staff have both fundamental and practical knowledge of such applications to geothermal reservoirs. This and other aspects of applied geothermal reservoir engineering have led to numerous communications with geothermal personnel of other countries interested in bi-national research projects to be administered by the National Science Foundation. One such study is in advanced stages of preparation. The Italian agency, ENEL, which produces geothermal steam at Larderello sent two Visiting Scholars, Dr. G. Manetti and Engr. A. Barelli, to Stanford during April and May, 1975, for special training in pressure transient analysis and planning exercises with the Stanford Staff. Other meetings and communications were held to plan joint research of fundamental importance *to* geothermal reservoir engineering.

During the current annual period, the initial research objectives of the geothermal chimney model were completed. Also completed were a study of the effect of temperature level on single-phase flow characteristics (to gas, liquid water, and mineral oil) of porous media; construction and testing of a batch physical geothermal model for capillary-pressure effect studies; calibration of a dielectric constant liquid content probe; an analysis of liquid content detection; a study of heat and mass transport within the pores of single particles, and a preliminary study of the thermal properties of fractured porous media. During the reporting period, work continued actively on development of mathematical models for the specific geothermal experiments within the program, development of new models of general and fundamental utility, field sampling for radon, and bench-scale flow experiments.

During the year, added emphasis was placed on chemical, geochemical, and environmental aspects of the laboratory experiments and potential field applications. Deposition of solids (dissolved from the porous media) in portions of the apparatus was observed and was a source of trouble from time to time. Chemical monitoring of the chimney model was instituted, and special analyses of deposits from bench-scale models were made.

THE CHIMNEY MODEL

The experimental efforts have been directed towards the study of highly fractured rock/water systems. It is visualized that the highly fractured region (chimney) is created artificially using proposed stimulation techniques such as hydraulic, thermal-stress, or explosive fracturing. Since the study of energy extraction from fractured rock is a major objective, fluid recharge was limited so that the energy addition by fluid recharge was generally less than energy extraction from the rock media. Part of the program consisted of the design and construction of a laboratory size model of a stimulated geothermal reservoir (the chimney model). This project was initiated during the latter part of 1972, and initial results were obtained in April, 1974. The design, construction, and initial checkout of the model has been described previously (Kruger and Ramey, 1973; and Kruger and Ramey, 1974).

A series of experiments with a rock loading consisting of approximately one inch equivalent diameter rocks has been completed. Preliminary results on the first nine experiments have been reported previously (Hunsbedt, Kruger, and London, 1975). Experiments with a second rock loading having larger equivalent diameter rocks and lower rock bulk porosity have also been completed. A few results on these experiments were presented earlier (Hunsbedt, Kruger, and London, 1975).

Efforts to model analytically and predict the observed transient behavior of the chimney model have been proceeding in parallel with the experimental efforts, and substantial progress has been achieved. Some highlights of the experimental and analytic efforts follow.

EXPERIMENTAL EFFORTS

Tests have been run with two different rock loadings. The first consisted of a gabbro rock* which had passed through a 1-1/2 inch (3.8 cm) square mesh. The second rock loading consisted of a true granite rock of considerably larger sizes than that of the first rock loading (largest rock was 38.2 lb(17.3 kg)).

To obtain information on the thermal behavior of the rocks for extrapolation to real systems, it is necessary to characterize the rocks used in the experiments. The rock size distributions were obtained by measuring the mass and the three orthogonal axes (length, breadth, and thickness) of individual rocks in random samples. These data were treated statistically to obtain the mean values and their standard deviations. Additionally, the data were used to compute other parameters such as the equivalent diameter, d, the shape factors breadth/length ratio, b/a, the thickness/length ratio, c/a, the roundness parameter, ψ, and surface area/volume ratio, A/V.

To extrapolate the behavior of the laboratory model reservoir to real stimulated reservoirs it is also necessary to know the rock loading bulk parameters, particularly the porosity. The drainage porosities for the two rock loadings were determined by filling the chimney void with water and measuring mass of water drained. From these measurements the mean solid densities of the rock were also determined. The permeabilities of both rock loadings were very large (no resistance to flow). The'intrinsic porosity of the rocks is considered very small compared to the drainage porosity, but no measurements were made. The rock loading characteristics are summarized in Table 1.

---

*The rock was available commercially as a "granite" rock. Closer examination revealed that a more appropriate designation was "Hornblende quartz gabbro."

TABLE 1

SUMMARY OF ROCK LOADING PARAMETERS

Parameter	First Rock Loading	Second Rock Loading
Rock Type	"Hornblende quartz gabbro"	"Granite"
Mean Equivalent Diameter, d	0.99 inch (2.52 cm)	2.65 (6.73)
Mean Thickness, c	0.74 inch (1.88 cm)	1.62 (4.11)
Thickness/length Ratio, c/a	0.50 dim. less	0.46
Mean Solid Density, ρ	174.3 lb_m/ft^3 (2.79 g/cm^3)	161.3 (2.61)
Drainage Porosity, ϕ	0.437	0.345

TABLE 2

RANGE OF TEST CONDITIONS AND PARAMETERS

QUANTITY	RANGE
Initial Pressure	255-796 psia (17.4-54.2 bar)
End Pressure	16-136 psia (1.1-9.3 bar)
Initial Temperature	386-500°F (197-260°C)
End Temperature	217-351°F (103-177°C)
Mean Steam Production Rate	2.4-56 lb_m/hr (1.1-25 kg/hr)
Mean Water Recharge Rate	0-28.1 lb_m/hr (0-12.7 kg/hr)
Mean Cool-down Rate	4.3-63°F/hr (2.4-35°C/hr)

A total of 29 runs has been made with the chimney model. The first three runs had water only in the chimney (100 percent porosity) and were made mainly for the purpose of establishing a reference for use in verifying the analytic model. Runs 4 through 25 were with the first rock loading (43.7 percent porosity). The early runs of this test series had no recharge while most of the later runs had recharge of either (1) cool water, (2) hot water with linearly decreasing inlet temperature, or (3) hot water at nearly constant inlet temperature. The last test series, runs 26 through 29, was with the second rock loading (34.5 percent porosity). Run 29 had recharge of hot water while the other runs of this test series had no recharge.

Other test conditions and parameters which could be controlled were varied over as great a range as was practical to provide the broadest possible experimental basis for analytic model verification. A summary of the range of test conditions and parameters of the experiments is given in Table 2.

An additional aspect of the chimney model tests was initiated early this year. The School of Earth Sciences is working with the USGS to determine the solubility of lithium present in small quantities in granite rock in geothermal systems. A number of water samples and samples of the rock used in the experiments has been obtained. All water analyses to date indicate that lithium is extracted from the rock in significant amounts (maximum concentration measured--300 parts per billion). These concentrations are one to two orders of magnitude greater than the initial concentration in the tap water charged. Concentration is a function of temperature and the length of time the water is in contact with the rock; it rises rapidly for the first few hours and then levels off.

ANALYTIC EFFORTS

An analytic model for the pressure/temperature transients of the chimney model has been developed. The two-phase steam mixture contained inside the control volume shown in Figure 1 is assumed to be at uniform temperature equal to the saturation temperature at the given pressure. Conservation of mass and energy leads to the following equation for the time derivative of pressure:

$$\frac{dP}{dt} = \frac{\dot{Q}_m + \dot{Q}_r + \left(i_i + v_f \frac{e_{fg}}{v_{fg}} - e_f \right) \dot{M}_i - \left(i_p + v_f \frac{e_{fg}}{v_{fg}} - e_f \right) \dot{M}_p}{\left[(e_f)' + \frac{V\phi}{M} \left(\frac{e_{fg}}{v_{fg}} \right)' - \left(v_f \frac{e_{fg}}{v_{fg}} \right)' \right] M}$$

where $e_{fg} = e_g - e_f$ = specific heat of vaporization (Btu/lb_m)

$v_{fg} = v_g - v_f$ = specific volume change (ft^3/lb_m)

M = mass of water in system at time t (lb_m)

$( )'$ = differentiation with respect to pressure (1/psia)

Other symbols are given in Figure 1. The quantities i_i, $\dot{M}_i$, i_p, and $\dot{M}_p$ are given functions of time based on experimental data or provided as input functions. The rock transient analysis is based on the assumption that the rock loading consists of spheres with three different equivalent diameters. The values of the rock diameters were based on the statistical rock size distribution data measured for the rock loadings. An energy balance on each rock size gives a set of first order linear differential equations for the mean temperature of the rocks in terms of the temperature of the surrounding two-phase steam mixture. The rate of heat transfer from the rocks, $\dot{Q}_r$, is computed from the product of the time derivative of the rock mean temperature, the rock mass, and the rock specific heat capacity.

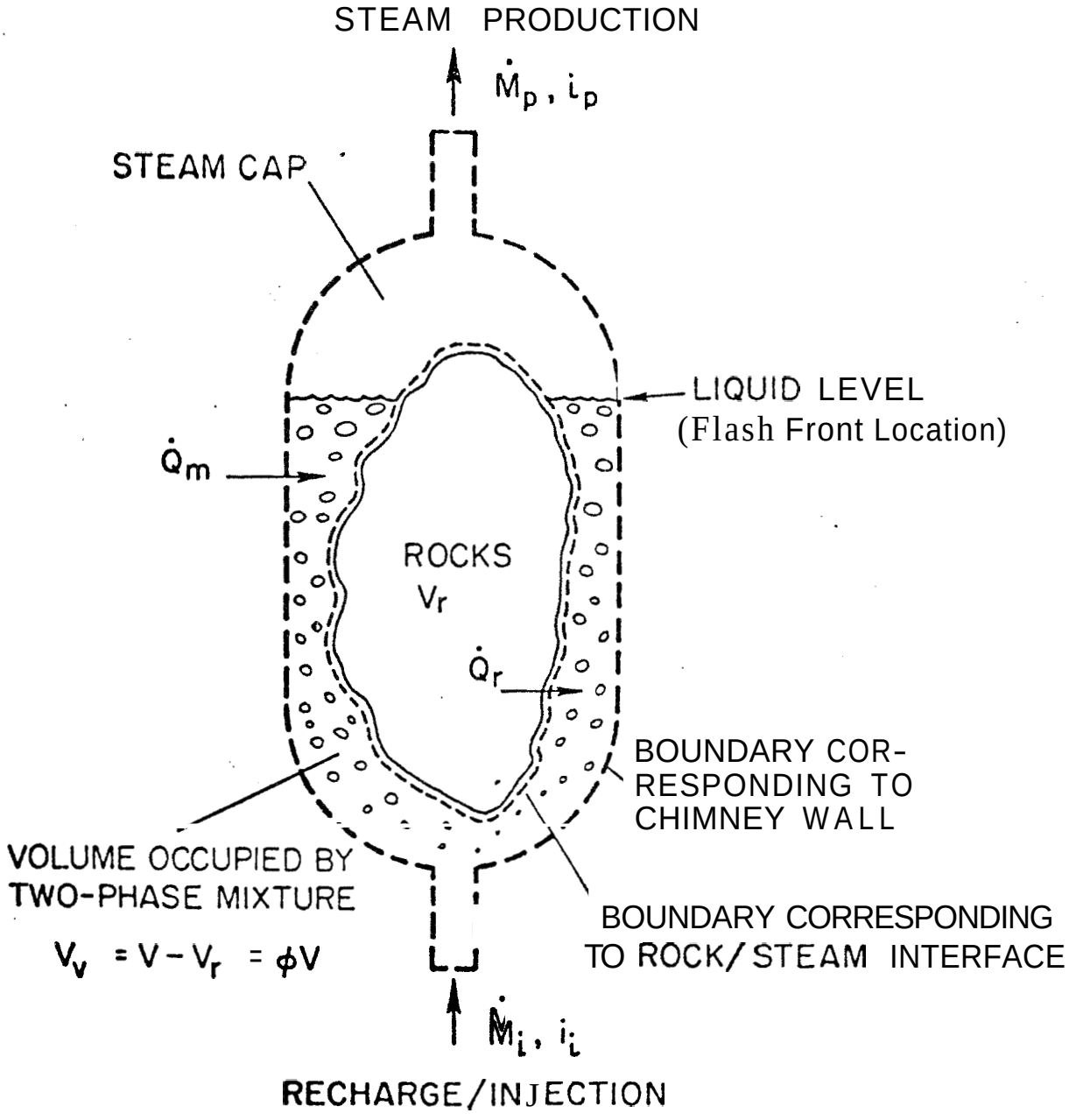

Figure 1. Control Volume for Analytic Modelling

The net energy transfer from the vessel (the wall effect) to the water/rock system under consideration is denoted by $\dot{Q}_m$. This energy transfer is derived based on an energy balance on the chimney metal and measured metal temperatures. An expression for $\dot{Q}_m$ has been given previously (Hunsbedt, Kruger, and London, 1975). The resulting system of equations can be solved numerically with given initial conditions and available equation of state data for the steam,*

SUMMARY OF RESULTS

The experimental results show that energy extraction from the rock is initiated upon pressure reduction so that flashing occurs in the chimney. The energy extraction from the rock is characterized by the rock energy extraction fraction, η, defined as the rock energy actually released to the energy available in the rocks between the temperature limits of the experiment. The rock energy extraction fractions achieved experimentally were generally higher than 75 percent and were found to depend mainly on the position of the liquid level in the chimney at the end of the experiment. The liquid level, in turn, depends on the recharge/production ratio, the end pressure, and the rock porosity. The maximum effect of rock size on η was less than 4 percent. Extrapolation of the results to a postulated full size, highly fractured system indicates that the average rock size can be one to two orders of magnitude larger than the average rock size normally found in chimneys produced by nuclear explosives (~1.5 ft) without affecting the rock energy extraction fraction to a significant degree.

The fraction of fluids originally in the chimney that can be produced, FP, depends strongly on the energy extraction from the rock and on

*The ASME formulations for the steam properties (McClintock and Silvestri, 1968) were used. Computer decks were made available by the Nuclear Energy Division of the General Electric Company, San Jose, California.

the rock porosity, ϕ. This is illustrated in Fig. 2 for initial and end pressures of run 26. These curves were computed from a mass-energy balance on the fluids in the chimney. For comparison, the point corresponding to the FP and η actually achieved for run *26* is also given in the figure. The actual fraction produced is higher than computed value by an amount δ, which is due to heat transfer from the metal wall.

The analytic model developed was used to predict the observed behavior of the reservoir. Input functions for $\dot{M}_p$, $i_{p'}$ and $\dot{Q}_m$ derived from the actual experiments were used. The predicted pressure transients for runs 3 and 26 (no recharge) are compared to the measured pressures" in Fig. 3. The agreement between experiments and prediction are excellent for these runs. The model was also tried for runs with recharge. It was found to work well if hot water was recharged, but in the case of cool water recharge the model predicted pressures lower than observed. The reason for this was that a zone of relatively low temperature water developed near the lower end of the chimney where the recharge took place. Further verification of the analytic model is in progress. A final report on the rock energy extraction experiments performed in the chimney model to date will be completed during the latter part of this year.

HARDWARE

The chimney model system has performed satisfactorily except that difficulties have been experienced with the large diameter O-ring used for sealing of the quick-opening head. However, a new high durometer reading O-ring (Viton) has been acquired which performs well at slightly derated maximum conditions ($\sim$485°F instead of 500°F and $\sim$650 psig instead of 800 psig). If additional problems with the O-ring require further

*The pressure is normalized to the initial saturation pressure. The non-dimensional time variable is the mean steam production rate divided by the initial mass in the system and multiplied by the transient time.

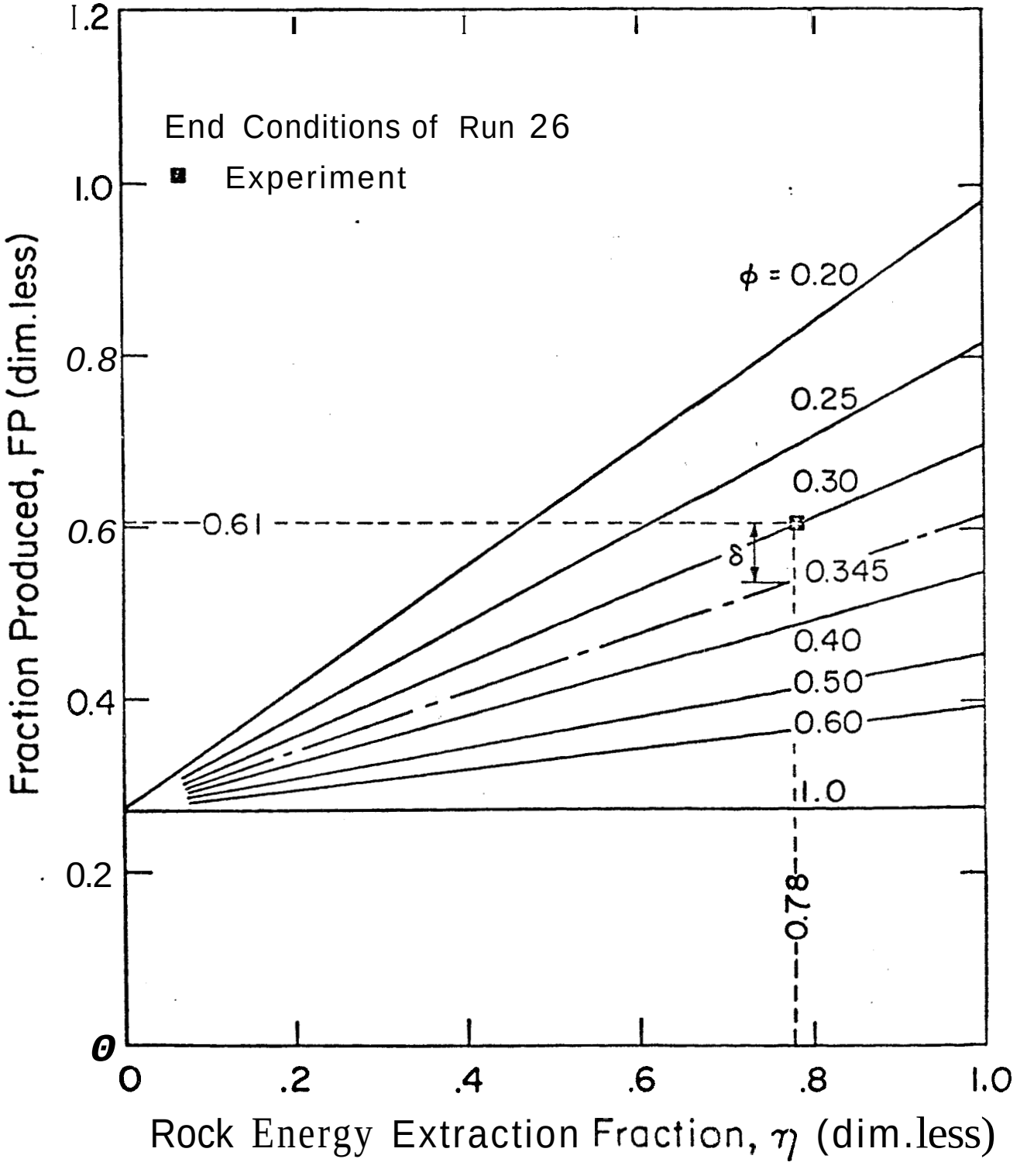

Figure 2. Fraction Produced vs. Rock Energy Extraction and Porosity

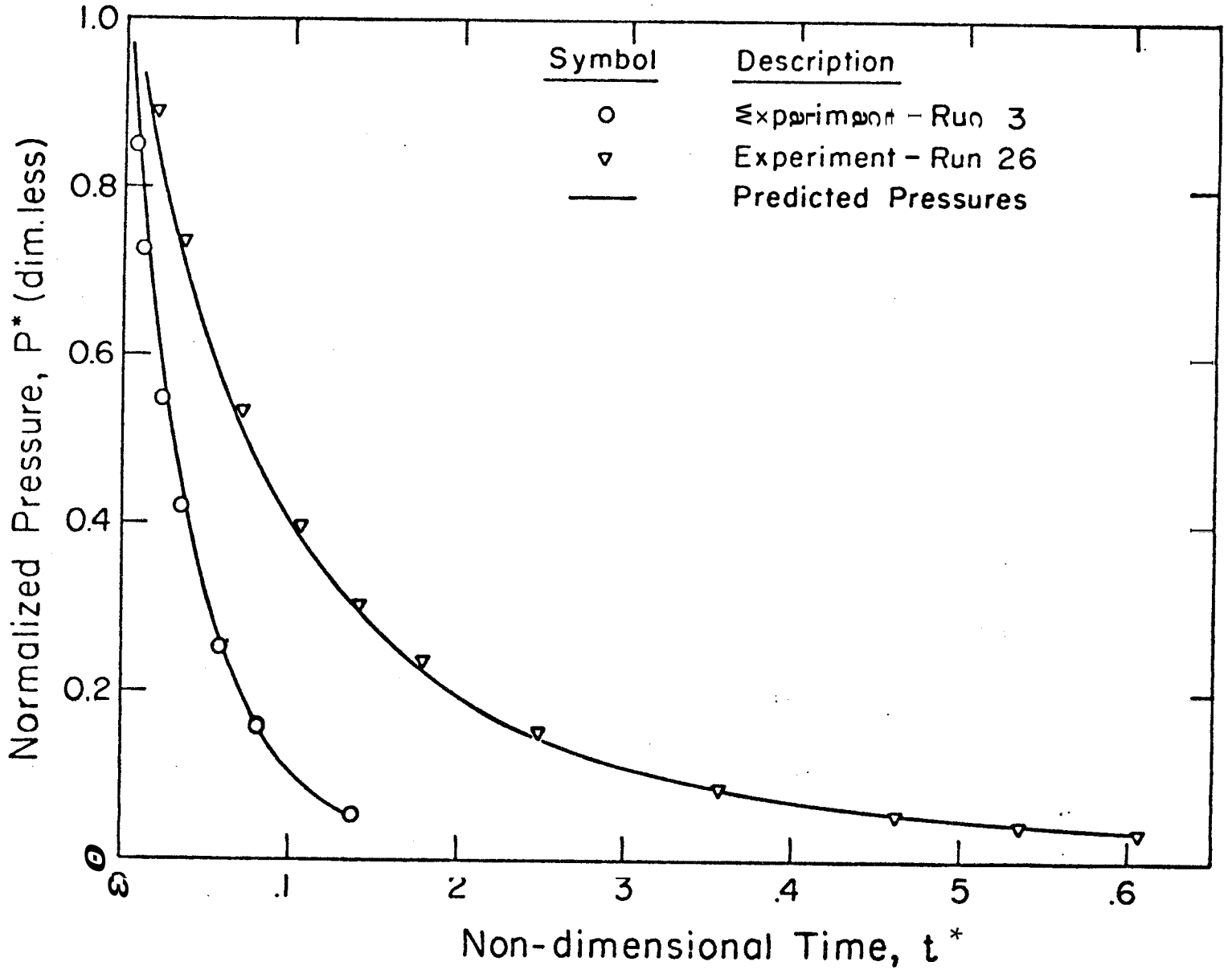

Figure 3 Comparison of Predicted and Experimental Pressure Transients with No Recharge

derating or corrective action, a plan for replacing the quick-opening head is being formulated.

Major problems were also experienced with the circulation pump seal. The seal mechanism usually fails after a few hours of operation due to deposits of silicates which precipitate from the cooler spots along the pump shaft. There seems to be no solution to this problem except replacing the pump, which is a major modification. Cleaning of the seal is now required after every experiment. Both the O-ring arrangement and the present circulation pump seal must be considered marginal and both place operational restrictions on the system.

Problems were also experienced with the injection pump, but it appears that this was caused by fouled valves. A set of new valves has been received, and during the last experiment no problems were experienced. It is anticipated that two piping components not installed during the construction phase due to lack of parts will be installed in the near future. Additional heating and heating control equipment is being considered for the tape heaters on the vessel.

FUTURE EXPERIMENTS

It is not expected that additional experiments with the second rock loading are required. The next planned experimental effort is with a rock loading from the Piledriver rubble chimney rock for heat transfer studies for microfractured rocks and for radio-tracer measurements of chemical characteristics of such rock-hot water systems.

BENCH-SCALE FLOW MODELS

The objectives and apparatus involved in the Bench-Scale Flow Models have been described in Progress Reports Nos. 1 and 3. During the current year, the first stage of the linear flow experiments was completed and described by Arihara, 1974.

The experiments were carried out by employing a Hassler-type core holder with cylindrical consolidated sandstones (24 inches long, 2 inches O.D.) in it. Both natural and synthetic cement-consolidated sand cores were used. Utilizing the same equipment, several different kinds of experiments were accomplished:

isothermal single-phase flow

non-isothermal single-phase flow, and

non-isothermal two-phase flow experiments.

The overall heat transfer coefficient for the core holder was measured in both hot fluid injection and cold water injection experiments, and compared with design calculations with good results. The steady-state overall heat transfer coefficient was found to depend on mass flow rate to a minor degree.

The thermal efficiency of hot water and cold water injection was found to depend on heat injection rate.

Two-phase boiling flow experimental data show that a significant decrease in both temperature and pressure can occur within the two-phase region, and that two-phase flow can be isenthalpic and steady state if heat transfer between the core and the surroundings is at a low level.

Experiments for the further study of the film coefficient at the surface of the core are being designed in order to investigate the rate dependency of the film coefficient.

A paper describing the present study was accepted for presentation at the 45th Annual California Regional Meeting, Society of Petroleum Engineers,

Ventura, California, April 3-4, 1975, and will be published in the Society of Petroleum Engineers Journal.

The Arihara work completed the initial phases of the linear flow Bench-Scale Model study. These phases included development of a method for construction of artificial sandstones to permit casting cores of low permeability and high porosity containing instrument probes, development of a suitable core holder which would permit instrumentation, and completion of initial runs for clean fluids and cores. One important component constructed by Arihara was a liquid content detector based upon the difference between the dielectric constant of steam and liquid water and employing a capacitance probe. Although Arihara demonstrated the principle, he did not calibrate the probe. During the current period, the bench-scale model effort has been focused in two important directions: (1) calibration of the liquid content probe, and (2) construction of a second model for parallel runs with boiling liquids containing salt in solution and gases in solution. The following will deal mainly with work on the liquid content probe. The development of this single instrument may be a major accomplishment.

Two pertinent reports follow. The first deals with work done directly with the bench-scale model. The second is a parallel study on liquid detection in porous media in general and the capacitance probe in particular,

BENCH-SCALE MODEL WORK WITH THE CAPACITANCE PROBE

The operating principle may be found in the "Liquid Saturation Probe" section of Progress Report No. 3 (June, 1974). The detailed diagrams of the capacitance probe, capacitance probe circuit and digital-to-analog converter circuit are shown in Appendix C of Arihara's dissertation. The capacitance (Baker, 1973) probe consists of three main components--probe, capacitance probe circuit, and digital-to-analog circuit. The sensitive portion of the capacitance

probe is really a construction of fringe capacitance. Such a fringe capacitance method has also been applied to measure the moisture content of soil in situ (Thomas, 1966). The capacitance probe circuit, which contains three important parts, is the most important portion. These three parts are (1) two crystal stabilized oscillators, (2) detector, and (3) amplifier. The two oscillators are identical except that one is connected with the capacitance probe. Both are tuned to about 7.5mHZ, with about 1.3 KHZ difference when the capacitance probe is immersed in air. Once set, the difference is fixed unless the capacitance of the probe changes. The schematic diagram of the apparatus used to measure liquid saturation is shown in Figure 4.

Akerlof and Oshry (1950) measured the static dielectric constant of water in equilibrium with its vapor over temperatures ranging from the boiling point (100°C) to the critical point (373°C). Their data fit the following equation:

$$E_{\sigma} = 5321T^{-1} + 233.76 - 0.9297T + 0.1417 \times 10^{-2}T^{2} - 0.8292 \times 10\text{-}6T3$$

where T is absolute temperature in °K.

The calculated values for dielectric constant of water at temperatures from 100°C to 240°C are shown in Table 3 and Figure 5. Warren (1962) indicated that the effect of pressure on dielectric constant is relatively small. The dielectric constant of water only changes 0.5% (or less) for each 100 psi change in pressure. The dielectric constants of steam at 100°C and 140°C are 1.0126 and 1.00785 respectively (Gray, 1963).

TABLE 3
COMPUTED VALUES FOR THE DIELECTRIC CONSTANT OF WATER AT TEMPERATURES BETWEEN 100°C AND 240°C

TEMPERATURE °C	E_o	TEMPERATURE °C	E_o
100	55.39	180	38.10
110	52.89	190	36.32
120	50.48	200	34.59
130	48.19	210	32.93
140	46.00	220	31.32
150	43.89	230	29.75
160	41.87	240	28.24
170	39.96		

For static calibration of the probe in the core filled with air and water, pyrex tubing (0.355 inch O.D.) was cast in the center of a synthetic core (80% sand, 20% cement by weight) with dimensions of 2.51 inches long and 1.93 inches diameter. The test core was heated to 310°F for three hours, evacuated, then water introduced to fully-saturate the core. The water saturation (content by volume) was calculated from:

$$S_w = \frac{W - W_d}{W_{sat} - W_d}$$

where S_w = water saturation, fraction of pore volume

W = weight of wet core, gm

W_d = weight of dried core, gm

W_{sat} = weight of fully saturated core, gm

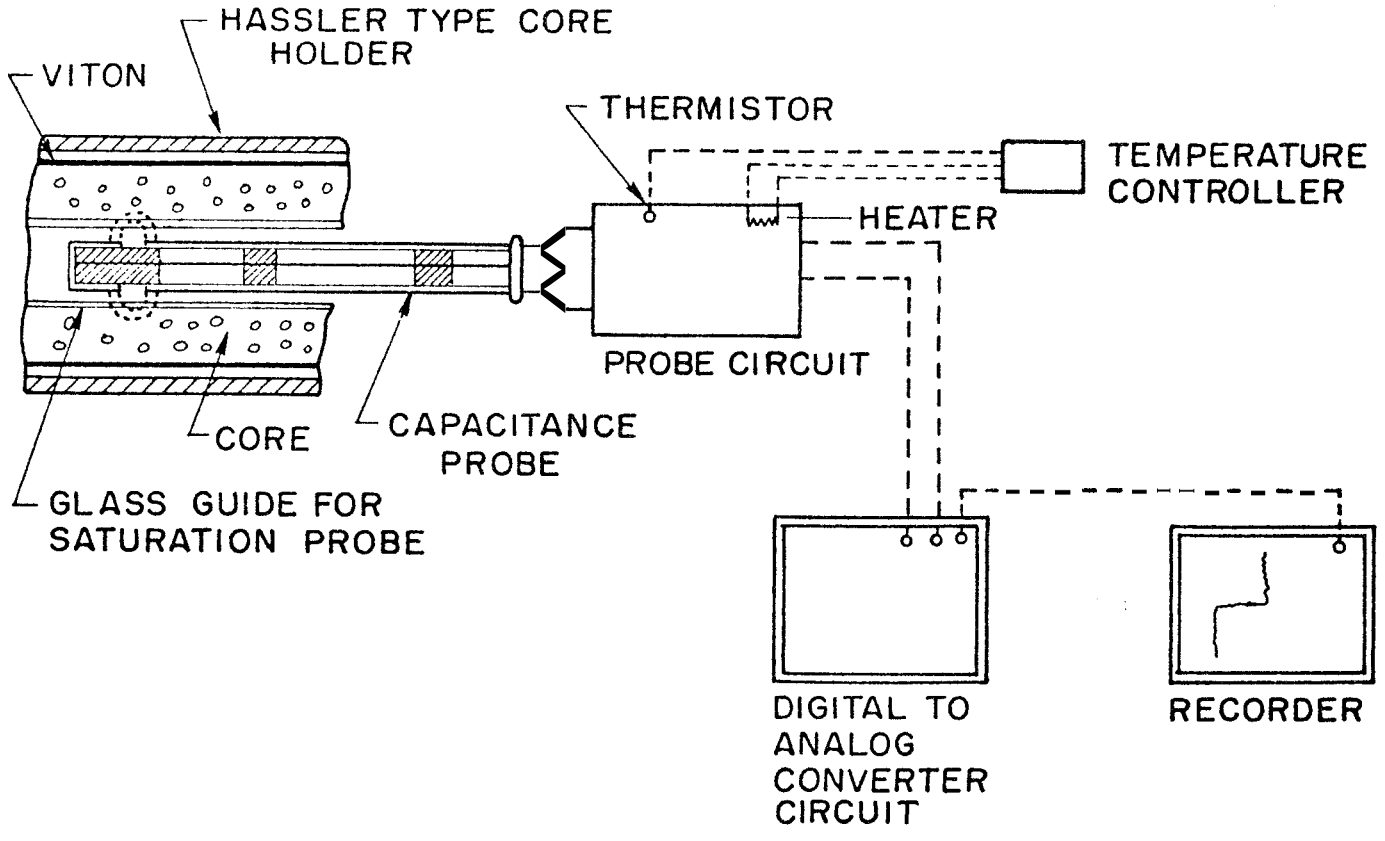

Figure C Schematic Diagram of the Measurement of Liquid Water Saturation in Porous Media

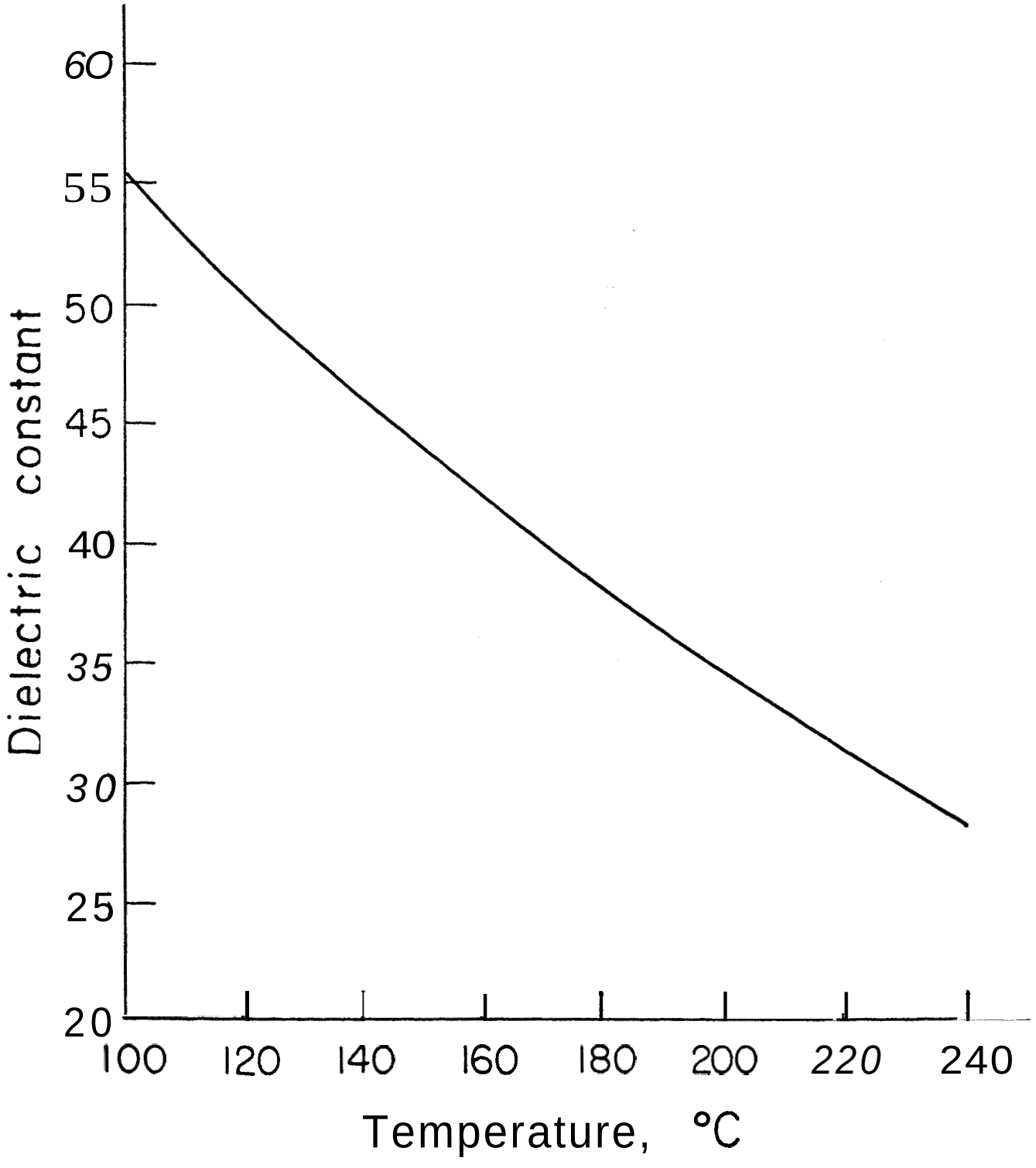

Figure 5. Computed Values for Dielectric Constant of Water vs. Temperature (Akerlof and Oshry. 1950)

There are two flow processes as fluids flow through porous media. These are the drainage and the imbibition processes. To simulate the drainage process, the fully saturated core is heated for different times to obtain different water saturations. For the imbibition process, the dried core is immersed in the water for different: times. The capacitance probe is inserted into the pyrex tubing as the tested core is in the core holder with Viton tube. The signal of the probe is recorded by a Heath recorder. The results are changed to mV by calculation. Typical results of such static testing are shown in Figure 6.

Steam-water calibration can be obtained by mass balance. The liquid water saturation in the core filled with steam and water can be calculated by:

$$S_w = \frac{V_w}{(\nu_s - \nu_w)} \left[\frac{\nu_s M}{V\phi} - 1\right]$$

where S_w = water saturation, fraction

ν_w = specific volume of water, cu ft/lb

ν_s = specific volume of steam, cu ft/lb

V = volume of the tested core, cu ft

ϕ = porosity of the core, fraction

M = total mass of the steam-water mixture in the core, lb

Since the dielectric constant of water decreases with temperature, the calibration curve for a steam-water system should consider the temperature as a parameter. The idealized calibration curve should look like Figure 7.

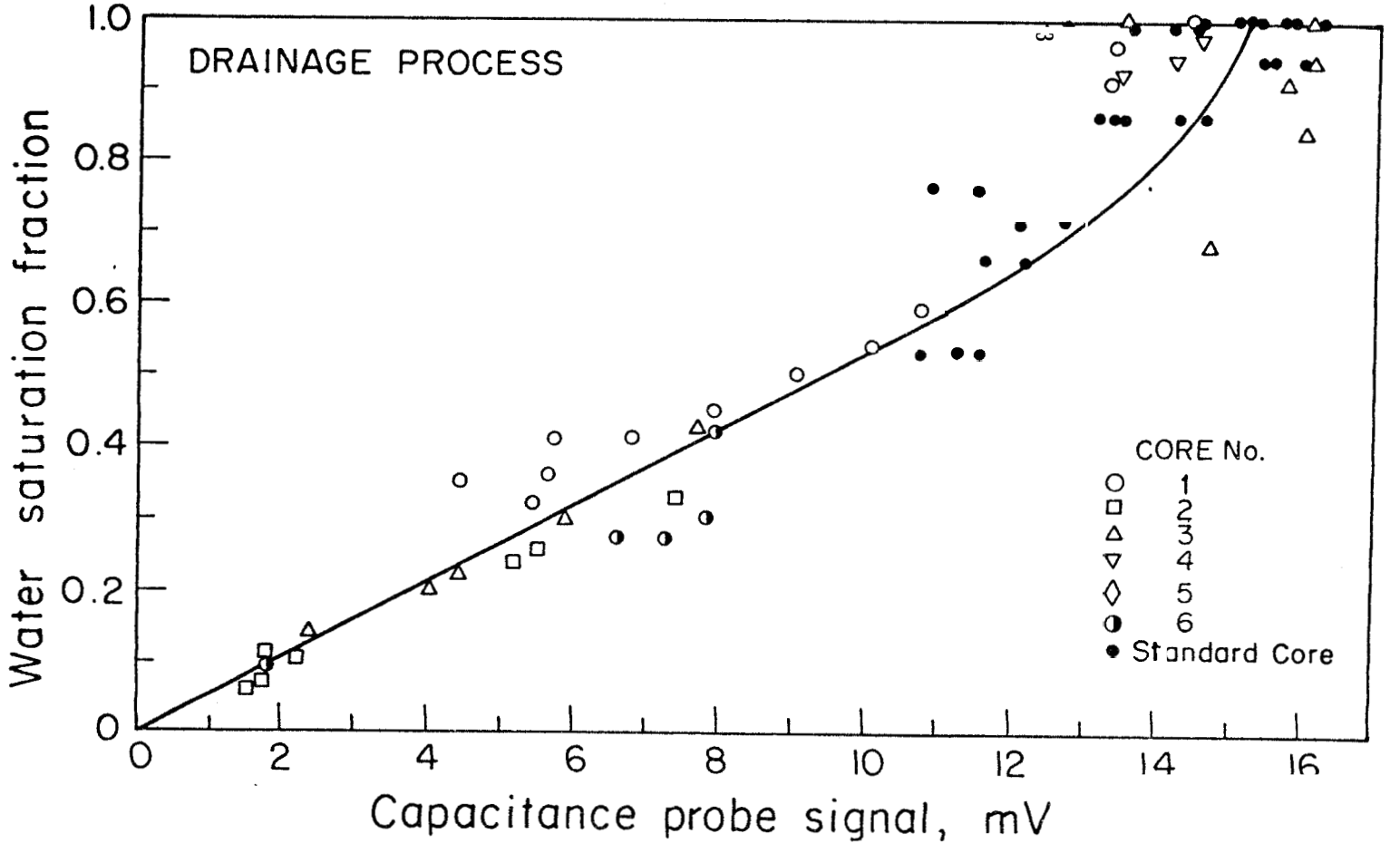

Figure 6. Capacitance Probe Output vs. Water Saturation in a Core Filled with Air and Water at Room Temperature (26°C)

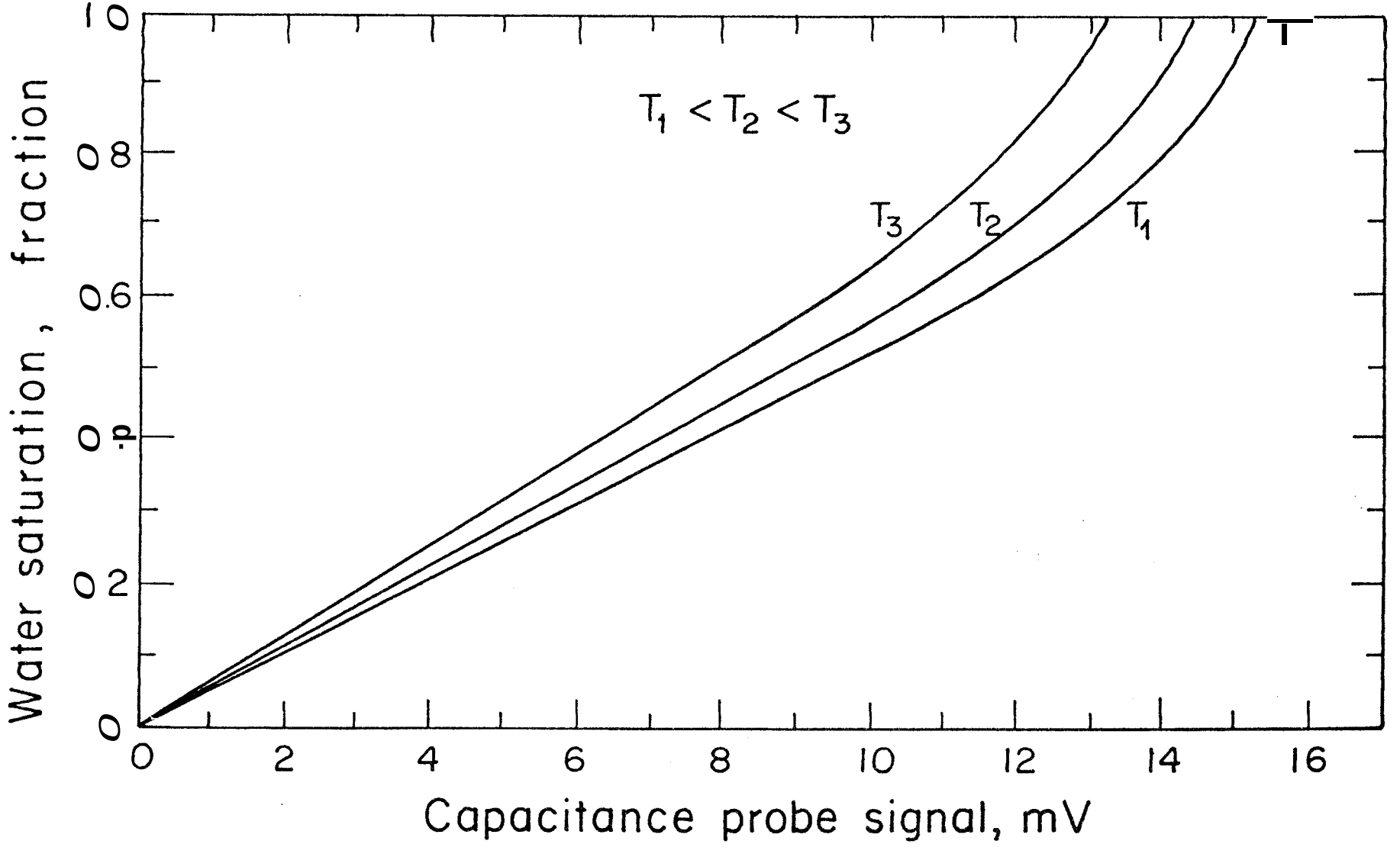

Figure 7. Idealized Capacitance Probe Output vs. Water Saturation in a Core Filled with Steam and Water

LIQUID DETECTION IN **POROUS** MEDIA

Although the Baker (1973) liquid probe had not been deveioped for geothermal system purposes and had not been calibrated, it appeared to have the characteristics required for the current program. Nevertheless, it appeared wise to review the existing methods, give liquid detection a fresh inspection, and examine the theory of dielectric constant probing in more detail. This project was undertaken and completed in the current period. Some of the results are presented by Denlinger (1975). The remainder will be presented in forthcoming studies by Chen. The following is a brief review of some important results.

The constraints which a probing device must satisfy are:

1. There must be a significant difference between the signal measured for water saturated porous media and that for steam saturated porous media.
2. The device must be able to measure a relatively narrow interval of core (2 - 3 cm or less) effectively.
3. The device must be able to be modified to fit the experimental conditions, such as a metal core casing and high temperatures and pressures.

The two most promising devices at present are both capacitance probes, which utilize the difference in dielectric constants between water and steam. One probe is already in use, the other is being considered. Two other methods which may prove applicable are:

(a) Nuclear magnetic resonance which measures the signal from precessing hydrogen nuclei in liquids.

(b) Ultrasonics, which measures the time of transit of a sonic impulse through the rock. The major problem with this method is detection of a sufficiently small interval in the core to inspect the details of two-phase flow.

Of all the methods studied to date, the capacitance probe comes closest to meeting the conditions of measuring liquid saturations in porous media at high temperatures and pressures. Theoretical analysis indicates that the dielectric constant (capacitance) probe detects changes within a depth of about one-sixth the core thickness--about *0.4* inches in the subject case.

VAPOR-PRESSURE LOWERING DUE TO CAPILLARITY

As volumetric liquid Saturations become very small within a porous medium, there is both a physical and a thermodynamic basis for expecting the vapor pressure to decrease due to interfacial tension effects. If such a phenomenon exists to a significant degree, flat surface (steam tables) vapor pressure data may not be appropriate for the conditions within a porous medium.

Such behavior has been studied by Ramey and co-workers since the late 1960's. Cady (1969) and Bilhartz (1971) concluded that the effect was not significant in unconsolidated sand reservoirs. Strobel (1973), on the basis of semi-quantitative corrections of experimental inaccuracies, appeared to have observed the lowering effect in a consolidated sandstone. The present ongoing work (Chicoine, 1975) is aimed at redesigning and rebuilding the experimental apparatus of Strobel *so* that the effect, if present, can be observed with greater accuracy.

During the current year, construction of the apparatus was completed and trial runs were made. Significant apparent vapor pressure lowering was observed (Chicoine, 1975). A detailed project report will be issued in the near future.

RADON IN GEOTHERMAL RESERVOIRS

The study of radon occurrence in geothermal reservoirs has been undertaken to evaluate the potential of radon as a diagnostic tool for studying the performance of geothermal reservoirs. An additional purpose was an evaluation of the environmental impact of radon release. The objectives of this study during the present year included three major tasks: 1) evaluate the potential environmental impact of radon release, 2) survey actual radon occurrence in different geothermal resource areas, and 3) establish a relationship between the radon concentration of the fluid and the flow rate of the well.

The method selected for measuring radon and the sampling techniques used have been described in "Radon Measurements in Geothermal Systems," Stoker and Kruger, **SGP-TR-4,** and are not discussed here.

ENVIRONMENTAL SAMPLING

A series of environmental atmospheric radon measurements were made in a mountain valley of the Geysers area of Northern California. Radon concentrations were measured in samples taken from ambient air and air near steam wells undergoing testing. The air samples were taken at three different locations in the valley. The first sampling point was at the lower end of the valley near hot springs. The second sampling point was approximately at the midpoint of the valley. The third sampling point was'at a ridge forming the upper boundary of the same valley. The samples were taken several times during a period of approximately one year.

In addition, several samples were taken near bleeding wells, and the prevailing winds, flow rate, and distance from the well were also recorded. The results are presented in Table 4.

TABLE 4

ENVIRONMENTAL, RADON MEASUREMENTS IN A MOUNTAIN VALLEY NEAR A GEOTHERMAL FIELD, THE GEYSERS, CALIFORNIA

AMBIENT AIR CONCENTRATIONS

DATE	LOCATION	RADON CONCENTRATION pCi/l
10 March 1974	Location 1	0.12 ± 0.01
18 May 1974	Location 1	< 0.07
14 Dec 1974	Location 1	0.14 ± 0.01
11 Jan 1975	Location 1	0.09 ± 0.01
18 May 1974	Location 2	0.11 ± 0.01
14 Dec 1974	Location 2	0.10 ± 0.01
11 Jan 1975	Location 2	0.13 ± 0.01
10 March 1974	Location 3	< 0.05
18 May 1974	Location 3	< 0.07
11 Jan 1975	Location 3	0.09 ± 0.01
17 Jan 1974	275 ft from well, still air	< 0.05
14 Dec 1974	250 ft from well, still air	0.09 ± 0.01
14 Dec 1974	230 ft downwind from well	0.15 ± 0.02
	World average (Johnson, 1973)	0.3

Natural air concentrations of ^{222}Rn may vary widely from one locale to another depending on the type of soil and atmospheric conditions. The average atmospheric content from 1 - 4 meters from the ground is 0.3 pCi/l; the maxima and minima are respectively 10 to 0.1 times that amount (Johnson et al., 1973; Eisenbud, 1963). As can be seen from the data, the concentrations obtained from the valley in the Geysers area are all below the world average by a factor of 2 - 3. The observed lower radon concentrations are consistent with the hypothesis that air masses reaching California from the Pacific Ocean are essentially radon free, and the emissions from the Geysers wells do not raise the radon concentration by a significant amount.

SURVEY OF RADON IN LARDERELLO, ITALY

One of the objectives of this study was to collect data on radon concentrations in different areas where geothermal resources are present. Five samples were taken from four different production fields in Larderello, Italy. Two samples were taken from a production well in the Larderello field, one sample was taken from the Castelnuovo, Serrazzano Pozzai, and Sasso Pissano fields. The results appear in Table 5 and Figure 8.

TABLE 5
RADON CONCENTRATION IN STEAM FROM LARDERELLO, ITALY

DATE	LOCATION	RADON IN CONDENSATE pCi/1
17 Feb 1975	Larderello	17,751 ± 700
17 Feb 1975	Larderello	36,833 ± 1,000
17 Feb 1975	Castelnuovo	32,511 ± 1,000
17 Feb 1975	Sasso Pissano	59,382 ± 1,500
17 Feb 1975	Serazzano Pozzai	18,012 ± 700

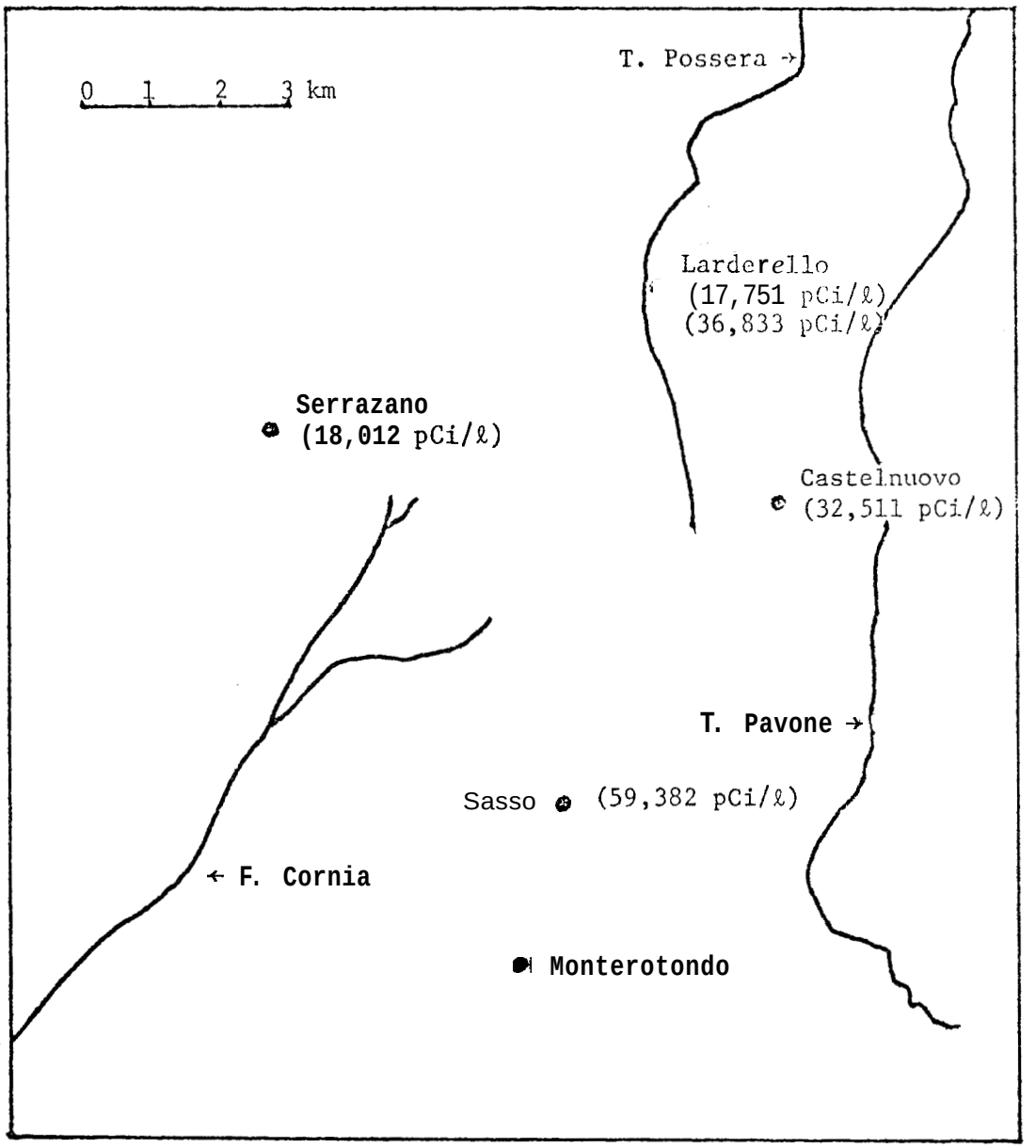

Figure 8. Larderello Geothermal Field. Radon Concentrations in Steam.

The radon concentrations in these samples were higher than those generally found in the Geysers area. The fraction of non-condensable gases is also higher in the Larderello field, with an average of five weight percent, compared with an average of 0.5 percent by weight found at the Geysers. A second set of samples from Italy has been arranged to test the reproducibility of consecutive samples, but the test has not been completed.

RADON EQUILIBRIUM AND RELATIONSHIP WITH FLOW RATE

Several experiments were conducted to attempt to gain a better understanding of the occurrence and behavior of radon in geothermal systems. Tests conducted in Wells I-A, I-B at the Geysers (Stoker, SGP-TR-4, page 98) indicated that the radon concentration was higher when the well was first opened and decreased to a steady state value. However, the variations from the average value were larger than could be attributed to error in measurements. Two different tests have been conducted to try to confirm the existence of a steady state. The first test consisted of sampling for a period of 18 hours. The results appear in Table 6.

TABLE 6
SUMMARY OF KESULTS
SAMPLING AT WELL II-B, GEYSERS AREA
JANUARY 11, 1975

Test started at 09:00 hours

Well Number	II-B	II-B	II-B
Time	13:00	17:00	19:00
Radon Content of Sample at Time of Collection	277.68	286.75	295.74
Amount of Condensate, ml	89 ± 2	96 ± 2	90 ± 2
Radon Concentration pCi/l	3120 ± 100	2799 ± 100	3286 ± 100

continued

Well Number	II-B	II-B	II-B
Time	21:00	01:00	03:00
Radon Content of Sample at Time of Collection, pCi	347.57	277.45	305.28
Amount of Condensate, ml	110 ± 2	93 ± 2	104 ± 2
Radon Concentration pCi/l	3159 ± 100	2983 ± 100	2935 ± 100

The results still show a larger variation than can be assigned to the errors in measurement and it is not known if these variations can be attributed to changes in the radon concentration of the steam sampled, or to unidentified errors in sampling or measurement. A similar problem has been encountered regarding the non-condensable gases in each sample. The amount of non-condensable gases may vary from sample to sample by a factor of two or even higher. It is not known if these samples are representative of the field conditions, or if non-condensable gases are escaping from the sample bottle through the bleed line. Tests should be conducted to determine the reliability of the sampling technique under use with respect to non-condensable gases. This can be done by taking a simultaneous sample, inducing condensation in the field and measuring the ratio of the volume of non-condensable gases to the volume of the condensate.

The second test, under way at the present time, consists of daily samples from a well for a period of three weeks, after which the flow rate is changed to half its initial value and daily sampling continues for another three weeks. This experiment has a twofold purpose. It will help evaluate the long-range variability of radon concentration and the dependence of radon concentration on steam flow rate. The results from the test will be useful for the evaluation of transient flow models.

Both heat and mass transfer mechanisms can contribute to energy extraction from fractured rocks as cold fluid is recycled to a stimulated geothermal reservoir. A mass transfer mechanism refers to the exchange between micropore water and macropore water. It is the objective of this study to investigate both heat and mass transfer phenomena from a single rock to the surrounding macropore water.

The synthetic rocks fabricated for the laboratory experiments are spheres. In heat transfer experiments a single rock, initially at a higher temperature, is immersed in a completely mixed tank of water, and the temperature of the water is recorded as a function of time. In mass transfer experiments, the spherical rock is initially saturated with tritiated water and immersed in a completely mixed tank of unlabeled water. The concentration of the tritiated water in the external water is recorded as a function of time.

Mathematical models have been prepared to represent the physical system, with heat transport models being similar to mass transport models. Heat transport is evaluated in terms of effective thermal diffusivity in the intrasphere region and in terms of the heat transfer film coefficient in the interface region. Mass transport is evaluated in terms of effective diffusivity in the intrasphere region and in terms of mass transfer film coefficient in the interface region. The mathematical models have been used to match the experimental data and to determine the value of effective diffusivity and film coefficients.

MATHEMATICAL MODELS

Derivation of a mathematical model of the experimental system for

heat transfer studies is similar to that for mass transfer studies. In this study, a derivation is presented for mass transfer studies only. A front model was developed last year and was described by Kruger and Ramey (1974), SGP-TR-1. A major objective has been to remove the pseudo-steady state assumption of the front model. In the following, the derivation of the analytical model is shown first. Numerical results for both the front model and the analytical model are then compared,

ANALYTICAL MODEL

In the mass transfer study, the system shown in Fig. 9 is considered. The system consists of two parts: (1) a porous sphere, the void space of which is filled with a solution of tritiated water, and (2) a surrounding fluid which is considered to have a uniform concentration. The system is subject to the following conditions:

(a) the initial concentration of the tritiated water in the porous sphere is uniform,

(b) the external solution always has a uniform concentration,

(c) the matrix of the porous sphere is inert, and

(d) the disintegration of tritiated water is negligible due to the long half-life of tritium, 12.4 years.

A mass balance of the tritiated water in the sphere leads to the following partial differential equation:

$$\frac{\delta C}{\delta t} = D_e \frac{1}{r^2} \frac{\delta}{\delta r} \left(r^2 \frac{\delta C}{\delta r} \right) \quad \text{.....(1)}$$

where C = the concentration of tritiated water

D_e = the effective diffusion coefficient of tritiated water

t = time

r = distance from center of porous sphere

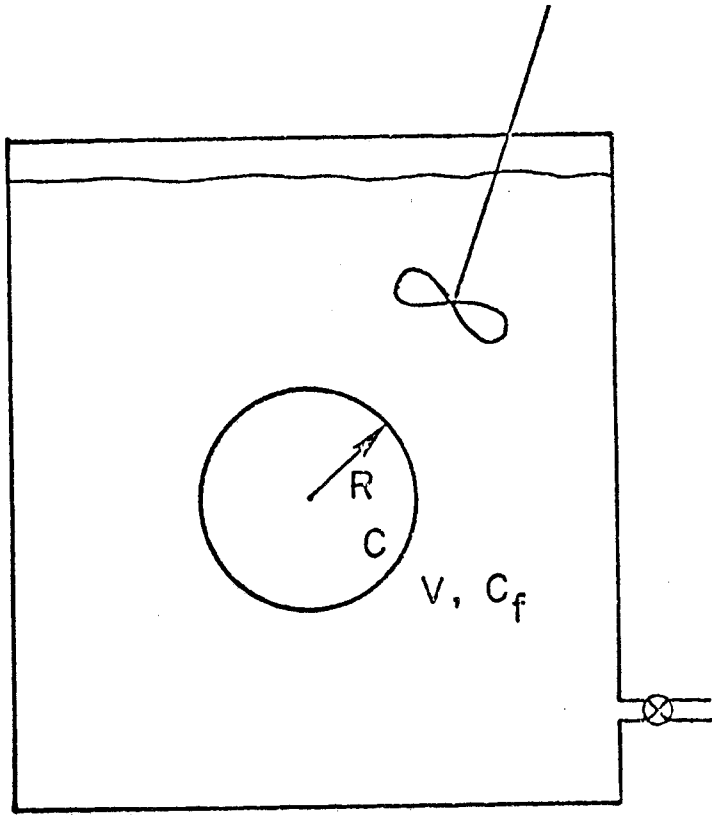

Figure 9. Schematic Diagram of Mass Transfer Experiment

A mass balance at the interface of the two parts gives:

$$V \frac{dC_f}{dt} = -D \left.\frac{\delta C}{\delta r}\right|_{r=R} A\phi \quad \text{.....(2)}$$

where R = the radius of the sphere

A = the surface area of the sphere, i.e., $4\pi R2$

C_f = the concentration of tritiated water in the surrounding fluid

ϕ = the porosity of the sphere

V = volume of the surrounding fluid

The initial and boundary conditions are as follows:

(a) the concentration within the porous sphere and that in the surrounding fluid are initially C_i and C_{fi}, respectively; that is,

when $t = 0$

$C = C_i$ for $r < R$

$C_f = C_{fi}$ for $r \geq R$

(b) at the interface between the sphere and surrounding fluid, the concentration is continuous; that is,

when $r = R$

$C = C_f$ for $t \geq 0$

For simplicity, the following set of dimensionless quantities is introduced:

$$X = \frac{C - C_i}{C_{fi} - C_i}$$

$$Y = \frac{C_f - C_i}{C_{fi} - C_i}$$

$$\theta = \frac{D_e t}{R^2} \quad \text{.....(3)}$$

$$\lambda = \frac{r}{R}$$

$$\alpha = \frac{RA}{V}$$

Substituting equation (3) into equations (1) and (2) gives:

$$\frac{\delta X}{\delta \theta} = \frac{1}{\lambda^2} \frac{\delta}{\delta \lambda} \lambda^2 \frac{\delta X}{\delta \lambda} \quad \text{.....(4)}$$

$$\frac{dY}{d\theta} = -\alpha \left. \frac{\delta X}{\delta \lambda} \right|_{\lambda=1} \quad \text{.....(5)}$$

The initial and boundary conditions become:

(a) when $\theta = 0$

$X = 0$

$Y = 1$

(b) at $\lambda = 1$

$X = Y$ for $\theta > 0$

A transformation $Z = \lambda X$ is introduced into equations (4) and (5). A set of two linear partial differential equations with constant coefficients are obtained.

$$\frac{\delta Z}{\delta \theta} = \frac{\delta^2 Z}{\delta \lambda^2} \quad \text{.....(6)}$$

$$\frac{dY}{d\theta} = -\alpha \left(\frac{\delta Z}{\delta \lambda} - Z \right)_{X=1} \quad \text{.....(7)}$$

The initial and boundary conditions become:

(a) when $\theta = 0$

$Z = 0$

$Y = 1$

(b) at $\lambda = 1$

$Z = Y$ for $\theta > 0$

(c) at $\lambda = 0$

$Z = 0$ for $\theta > 0$

The Laplace transformation of equations (6) and (7) and the initial and boundary conditions with respect to 6 yields:

$$S\bar{Z} = \frac{d^2\bar{Z}}{d\lambda^2} \quad \text{.....(8)}$$

$$S\bar{Y} - 1 = -\alpha\left(\frac{d\bar{Z}}{d\lambda} - \bar{Z}\right)\Big|_{X=1} \quad \text{.....(9)}$$

(a) $\bar{Z}(S,1) = \bar{Y}(S)$

(b) $\bar{Z}(S,0) = 0$

Solving equation (8) with boundary condition (b) leads to:

$$\bar{Z} = 2a_1 \sinh (s^{1/2}\lambda) \quad \text{.....(10)}$$

where a_1 is a constant, and can be determined through equation (9) and boundary condition (a) as follows:

$$a_1 = \frac{1}{2\left[(s - \alpha) \sinh (s^{1/2}) + \alpha s^{1/2} \cosh (s^{1/2})\right]} \quad \text{.....(11)}$$

Combining equations (10) and (11) gives:

$$\frac{\sinh (s^{1/2}\lambda)}{\left[(s - \alpha) \sinh (s^{1/2}) + \alpha s^{1/2} \cosh (s^{1/2})\right]} \quad (12)$$

Employing the transformation, $\bar{Z} = \lambda\bar{X}$, and equation (12), $\bar{X}$ can be written as:

$$\bar{X}(S,\lambda) = \frac{\sinh (s^{1/2}\lambda)}{\alpha\lambda\left[(\frac{s}{\alpha} - 1) \sinh (s^{1/2}) + s^{1/2} \cosh (s^{1/2})\right]} \quad \text{.....(13)}$$

$$= \frac{\sinh (s^{1/2}\lambda)/\sinh (s^{1/2})}{\alpha\lambda\left[(\frac{s}{\alpha} - 1) + s^{1/2} \coth (s^{1/2})\right]} \quad \text{.....(14)}$$

The inverse Laplace transforms of $\bar{X}$ can be obtained by means of the residue theory,

$\bar{X}(s,\lambda)$ has a first order pole at S = 0. Moreover, $\bar{X}(s,\lambda)$ has an infinite number of first: order poles, namely, the points where

$$\frac{s}{a} - 1 + s^{1/2} \coth (s^{1/2}) = 0$$

or, the points where $S = -\gamma_n^2$, and γ_n satisfies

$$\gamma_n \cot \gamma_n = 1 + \frac{\gamma_n^2}{a}$$

and, $n = 1, 2 \ldots, \infty$

at $S = 0$ the residue is

$$\lim_{s \to 0} \frac{s \sinh\left(s^{1/2}\lambda\right) e^{s\theta}}{\alpha\lambda \left[\left(\frac{s}{\alpha} - 1\right) \sinh\left(s^{1/2}\right) + \cosh\left(s^{1/2}\right)\right]} = \frac{3}{\alpha + 3}$$

at $S = -\gamma_n^2$ the residue is

$$\lim_{s \to -\gamma_n^2} \frac{\left(s + \gamma_n^2\right) e^{s\theta} \sinh\left(s^{1/2}\lambda\right)/\sinh\left(s^{1/2}\right)}{\alpha\lambda \left[\left(\frac{s}{\alpha} - 1\right) \sinh\left(s^{1/2}\right) \cot\left(s^{1/2}\right)\right]}$$

$$= \frac{2\, e^{-\gamma_n^2 \theta} \sin(\gamma_n \lambda)/\sin(\gamma_n)}{\lambda \left[\left(\alpha + \quad + \frac{\gamma_n^2}{\lambda}\right]\right.}$$

Hence, the inverse Laplace transform of $\bar{X}(S, \gamma)$ can be obtained by summing the above residues:

$$X(\theta, \lambda) = L^{-1}\left\{\bar{X}(S, \lambda)\right\}$$

$$= \frac{}{\alpha + 3} + \frac{2}{\lambda} \sum_{n=1}^{\infty} \frac{\sin(\gamma_n \lambda)}{\sin(\gamma_n)} \frac{e^{-\gamma_n^2 \theta}}{\left[(\alpha + 3) + \frac{\gamma_n^2}{\alpha}\right]} \quad \ldots\ldots\ldots\ldots (15)$$

$Y(\theta)$ equals $X(\theta, \lambda)$ when $\lambda = 1$, and can be written as follows:

$$Y(\theta) = \frac{3}{\alpha + 3} + 2 \sum_{n=1}^{\infty} \frac{e^{-\gamma_n^2 \theta}}{\left[(\alpha + 3) + \frac{\gamma_n}{\alpha}\right]} \quad \ldots\ldots\ldots\ldots\ldots\ldots\ldots\ldots (16)$$

COMPUTATIONAL RESULTS

Both the front and analytical models were simulated by computer. The parameters involved in the model were estimated based on the laboratory experimental system, preliminary experimental data, and the literature available. The numerical values for the parameters were as follows:

$$R = 1.00 \text{ in.}$$

$$\phi = 0.20$$

$$V = 3.00 \text{ liter}$$

$$D = 2.44 \times 10^{-5} \text{ cm}^2/\text{sec.}$$

$$D_e = \frac{D}{2} = 1.73 \times 10^{-5} \text{ cm}^2/\text{sec.}$$

The simulation results for tritiated water concentration in the surrounding fluid, Y, with respect to time, θ, are shown in Figure 10. The results indicate that the front model does not represent the system well, especially for long periods of time. The simulation results also suggest that the surrounding concentration is almost constant. Efforts are being made to incorporate the film coefficient in the mathematical model by assuming constant concentration in the surrounding fluid,

MASS TRANSFER EXPERIMENTS

Preliminary mass transfer experiment results are shown on Figs. 11 and 12. Figure 11 shows the soaking curve of the synthetic spherical rock in water. It can be seen that after four hours of soaking, the weight of the sphere saturated with water was almost constant. In the tritiated water tracer experiment, the sphere was saturated in the same way and immersed in a completely mixed tank of water. The concentration of tritiated water was measured by a liquid scintillation counter as a function of time as shown in Fig. 11. The experimental data were matched with

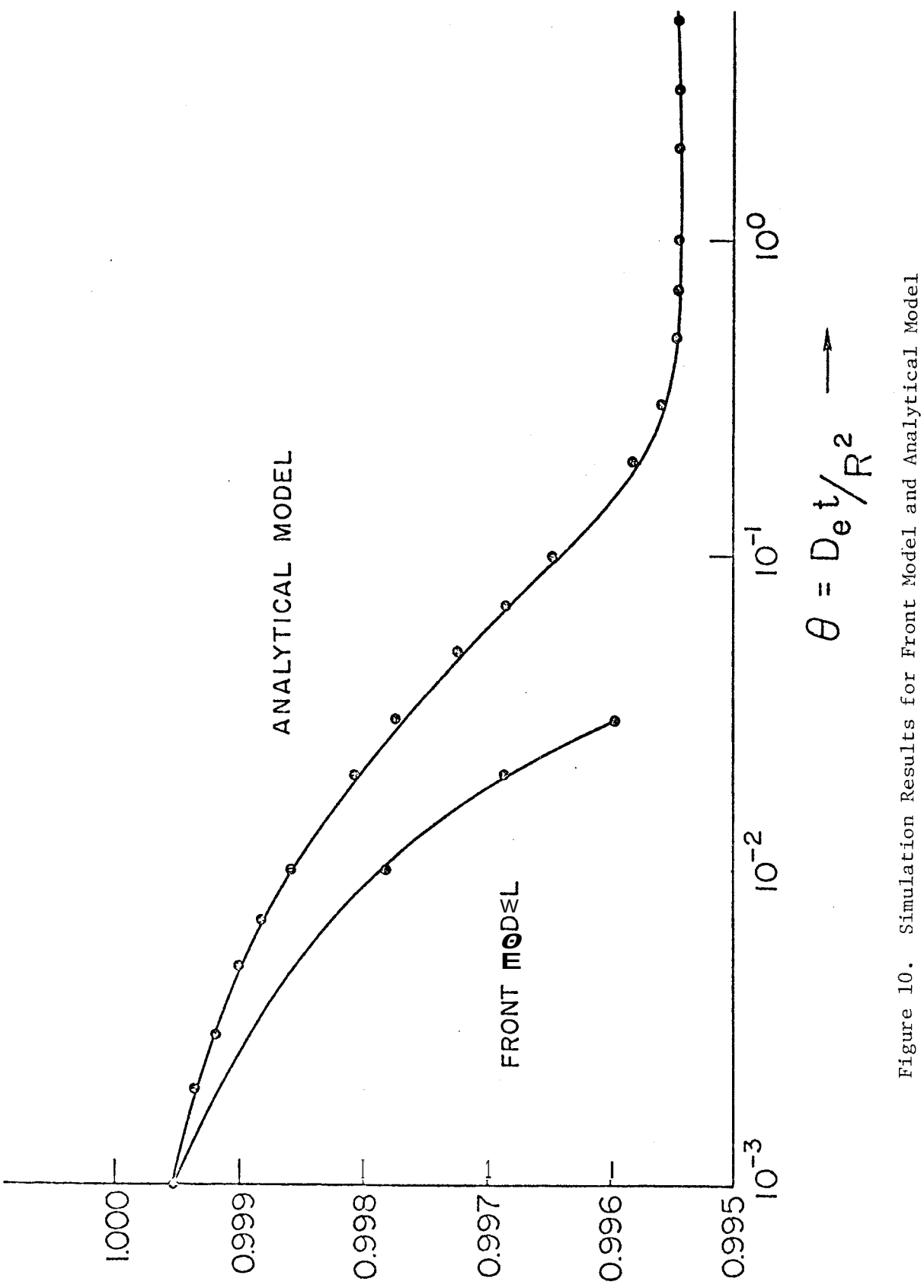

Figure 10. Simulation Results for Front Model and Analytical Model

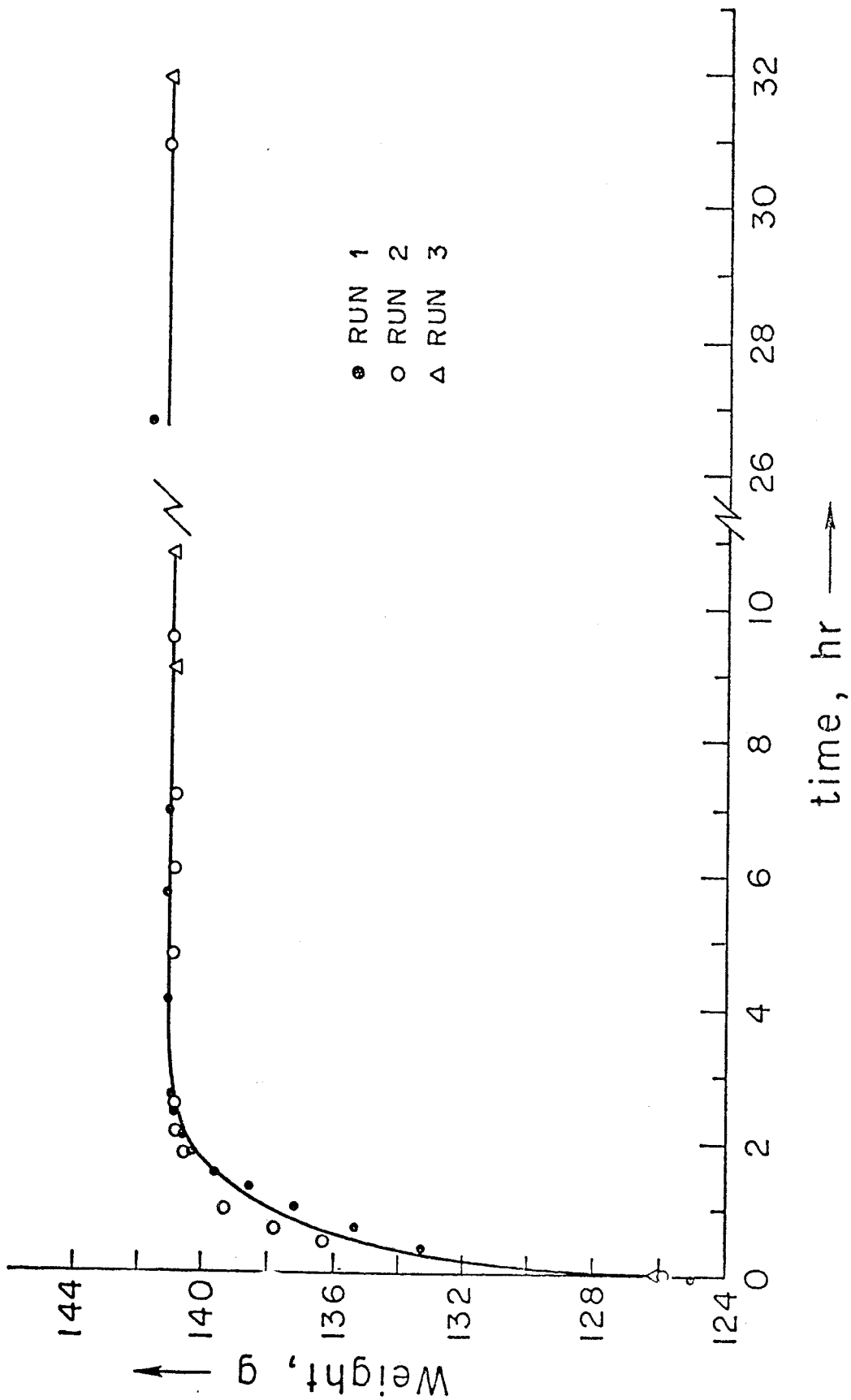

Figure 11. Soaking Curve

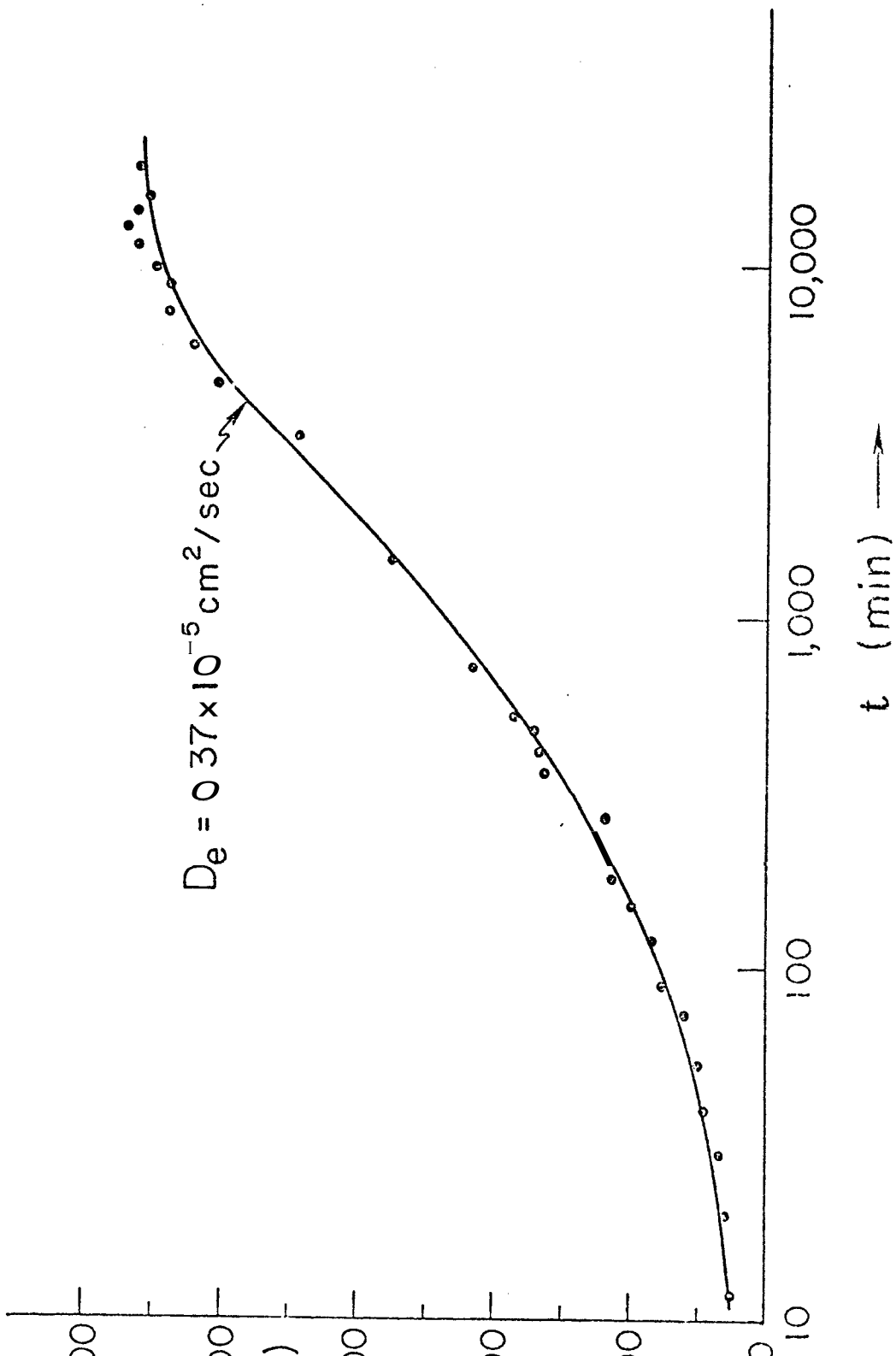

Figure 12. Mass Transfer of Tritiated Water from a Porous Sphere to Surrounding Fluid

a mathematical model. The effective diffusivity of tritiated water in the synthetic spherical rock was evaluated to be 0.37×10^{-5} cm^2/sec. This value is in the same order as the molecular diffusivity of tritiated water. Therefore, it is concluded that the mass transport mechanism in the intrasphere region is mainly molecular diffusion. Further experiments are to be run under rigorous temperature control.

HEAT TRANSFER EXPERIMENTS

The schematic diagram of heat transfer studies is shown in Fig. 13. Before conducting transient heat transfer experiments, it was necessary to calibrate the heat loss from the experimental system, which was insulated from the environment by polystyrene foam. The experiments were made for this purpose. A simplified "lumped parameter" analysis of the problem was made, in which the various masses of water and glass were considered to be at uniform temperature.

The mathematical model for cooling experiments was obtained from an energy balance for the experimental system, i.e.,

$$MC \frac{dT}{dt} = -hA\ (T - T_\infty)$$

where MC = heat capacity of the experimental system

T = temperature of the system

T_∞ = temperature of the environment

hA = heat transfer coefficient-area product for the system

Solving the above equation with the initial condition $T = T_i$ at $t = 0$ yields

$$\ln (T - T_\infty) = -\frac{hA}{MC} + \ln (T_i - T_\infty)$$

Experimental results are shown in Figs. 14 and 15. The heat transfer coefficient-area product for the system can be found from the slope, and is about 0.6 to 0.7 BTU/hr-°F. Future efforts will be

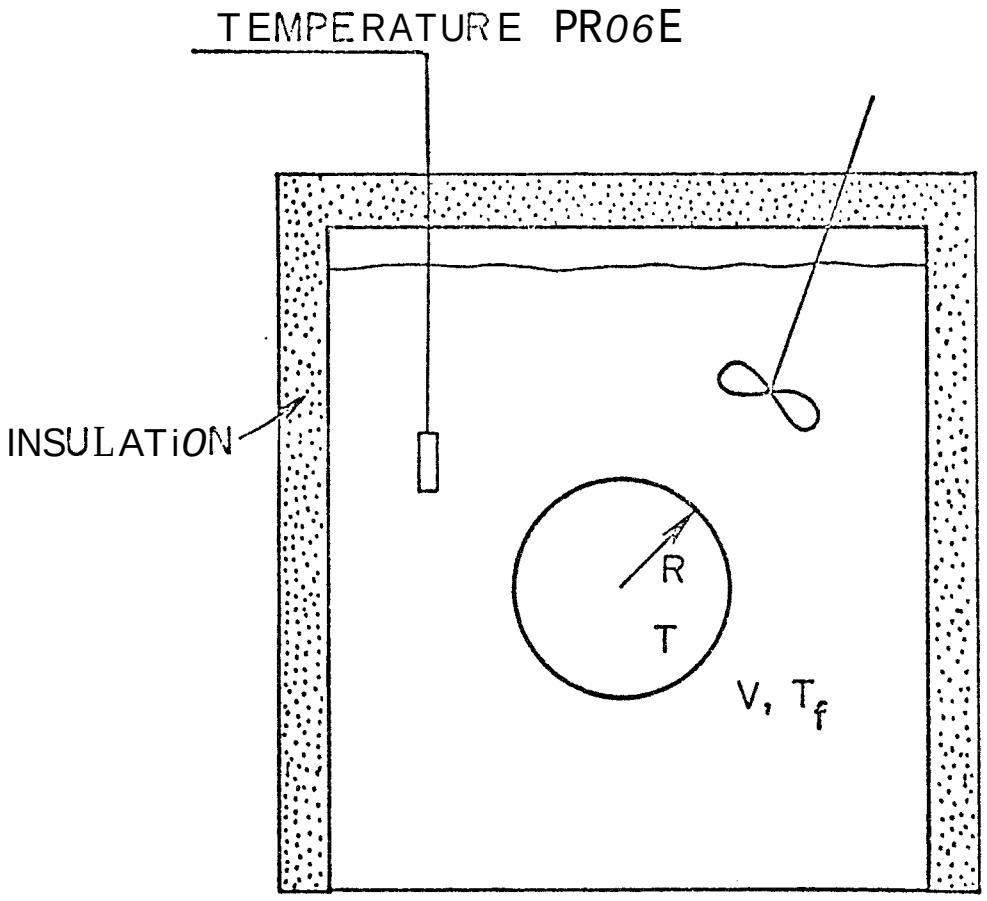

Figure 13. Schematic Diagram of Heat Transfer Experiment

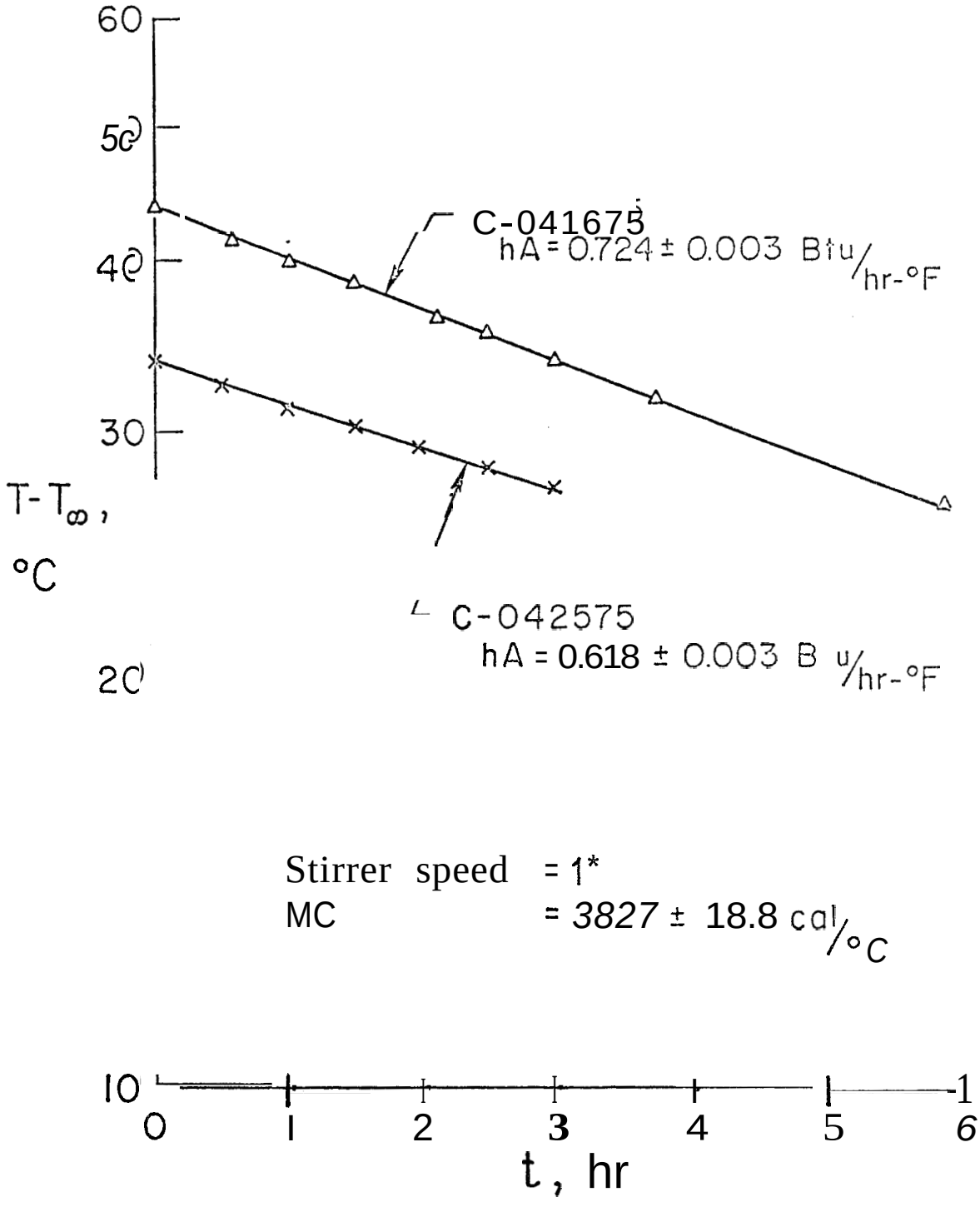

Figure 14. Cooling Heat Transfer Experiment

*Note: Stirrer Speed 1 is a rheostat setting on the mixer.

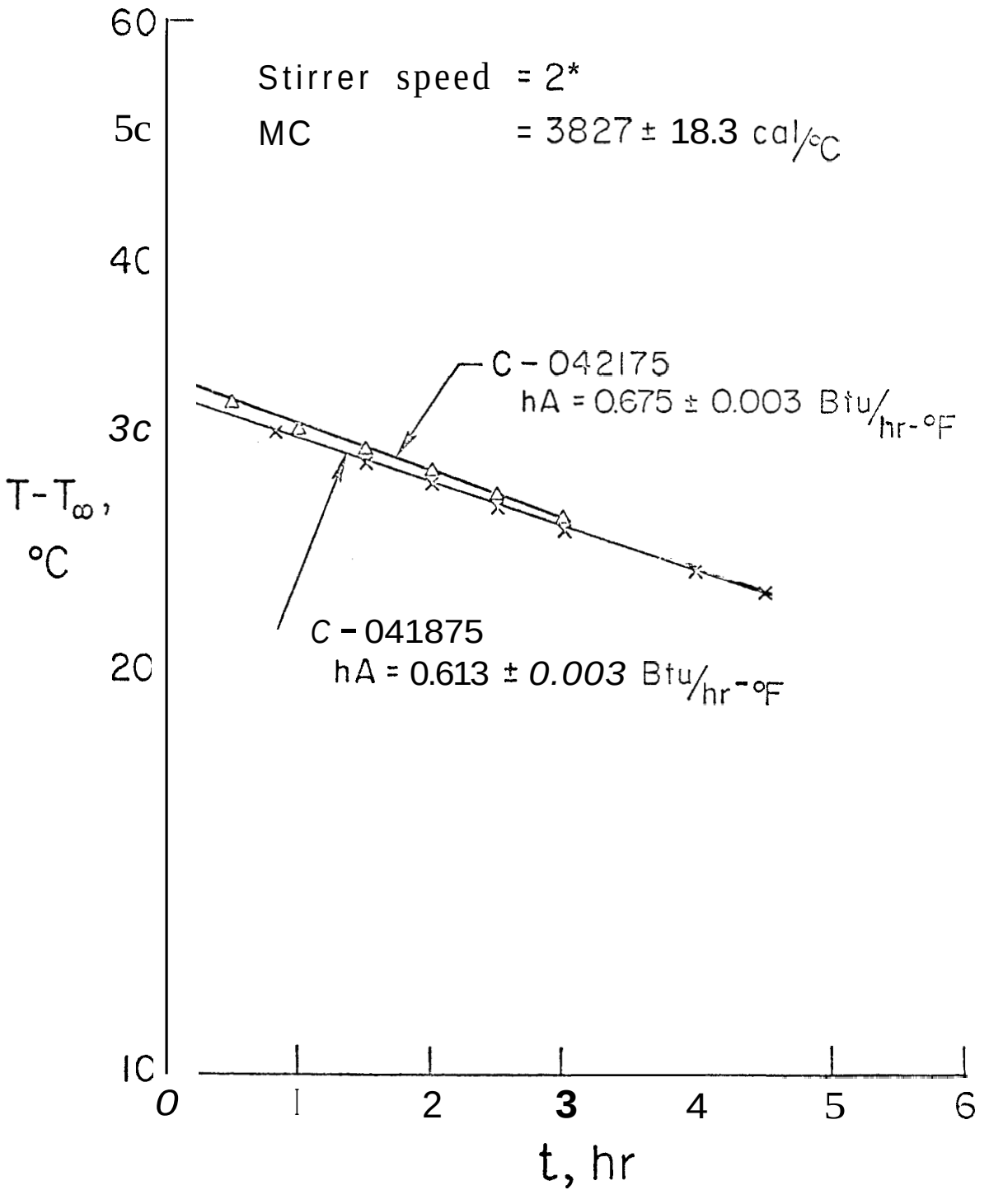

Figure 15. Cooling Heat Transfer Experiment

*Note: Stirrer Speed 2 is a rheostat setting on the mixer.

directed to a study of the heat transfer from the sphere to the external fluid.

The rate equation for heat transfer from the sphere to water can be expressed as:

$$q = hA\ (T_s - T_w)$$

The energy balance for the water can be written as:

$$C_w \frac{dT_w}{d\theta} = 4$$

A combination of the energy balance and the rate equation results in:

$$C_w \frac{dT_w}{d\theta} = hA\ (T_s - T_w) \quad \text{.....(17)}$$

where C_w = heat capacity of water

T_w = temperature of water

T_s = temperature of sphere

hA = heat transfer coefficient-area product

θ = time

Assuming the experimental system is isolated from the surroundings, the following result is obtained:

$$C_w\ (T_w - T_{wi}) = C_s\ (T_{si} - T_s) \quad \text{.....(18)}$$

where C_s = heat capacity of the sphere, and

T_{wi} = initial temperature of water

T_{si} = initial temperature of the sphere

From equation (18)

$$T_s = \frac{w}{C} (T_w - T_{wi}) + T_{si}$$

Let $\frac{1}{C_s^*} = \frac{C_w}{C_s}$

Thus : $$T_s = -\frac{1}{C_s^*} (T_w - T_{wi}) + T_{si} \quad \text{.....(19)}$$

Substituting equation (19) into (17) yields:

$$C_w \frac{dT_w}{d\theta} = hA \left[(T_{si} - a(T_w - T_{wi}) - T_w \right] \quad \ldots\ldots(20)$$

Rearranging equation (20) yields:

$$C_w \frac{d(T_w - T_{wi})}{d\theta} = -hA\left(\frac{1}{C_s^*} + 1 \right) (T_w - T_{wi}) + hA\,(T_{si} - T_i) \quad \ldots\ldots(21)$$

Let $T_w^* = \frac{T_w - T_{wi}}{T_{si} - T_{wi}}$ and equation (21) becomes:

$$\frac{dT_w^*}{d\theta^*} + \frac{hA\left[\left(\frac{1}{C_s^*} + 1 \right)\right]}{C} T^* \quad \frac{hA}{} \qquad (22)$$

Let $\theta^* = \frac{hA\theta}{C_w}$ and equation (22) becomes:

$$\frac{dT}{d\theta} + \left(\frac{}{*} + 1 \right) = 1 \quad \ldots\ldots(23)$$

subject to $T_w^* = 0$ at $\theta^* = 0$.

Solving equation **(23)** with the above initial condition gives:

$$T_w^* = \frac{1}{\frac{1}{C_s^*} + 1} \left[1 - e^{-\left(\frac{1}{C_s^*} + 1 \right) \theta^*} \right]$$

or $$\ln \left\{ \frac{1 - \left(\frac{1}{C^*} + 1 \right) T_w^*}{} \right. \quad - \quad = - \left(\frac{1}{C_s^*} + 1 \right) \theta^*$$

s

or $$\ln \left[\frac{1}{C_s^*} - T_w^* \right] \approx \frac{-hA}{C_s} \theta \quad \ldots\ldots(24)$$

The experimental results are plotted on Figure 16 and are matched with equation (24). "h" is estimated as 141.1 BTU/ft^2hr for the first thirty seconds, and as 214.2 BTU/ft^2hr for the latter thirty seconds. The change indicates that a more sophisticated parametric model must be developed. Type curves will be developed to match the data shown in Fig. 17, and used to evaluate the thermal conductivity of the rock sphere.

Preliminary experiments have been conducted for both mass transfer and heat transfer from a single porous rock to the surrounding fluid. Energy transfer due to both heat and mass transfer mechanisms were analyzed. The transport process may be divided into two steps: (1) intrasphere transport, and (2) interface transport. It appears that heat transfer is the dominant mechanism for energy transfer from a hot porous sphere *to* the surrounding fluid.

INTRASPHERE TRANSPORT

Heat transfer inside the porous sphere is primarily carried out by conduction in the micropore water and the rock matrix. An "effective thermal conductivity" may be used for this mechanism. This intrasphere effective conduction process can be described by:

$$\frac{\partial T}{\partial \theta} = a \frac{1}{r^2} \frac{\partial}{\partial r} \left(r^2 \frac{\partial T}{\partial r} \right) \quad \text{.....(25)}$$

where T = temperature,

a = effective thermal diffusivity of porous sphere saturated with water,

θ = time, and

r = distance from center of porous sphere.

The mass transfer inside the porous sphere is mainly due to molecular diffusion of the micropore water. The rate of this process can be characterized by a parameter, D_e, which is the effective diffusivity. This intrasphere

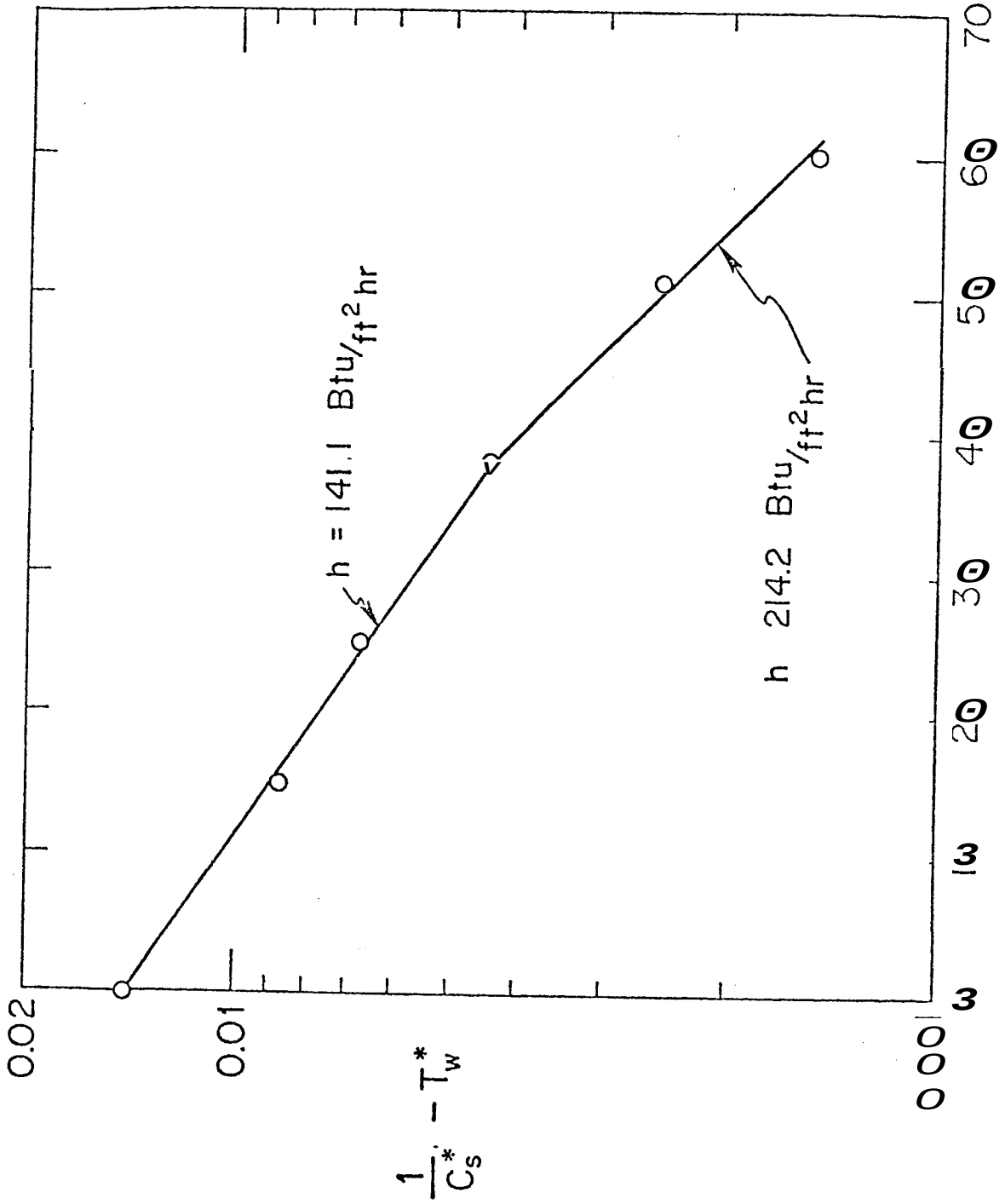

Figure 16. Heat Transfer from a Porous Sphere to the Surrounding Fluid

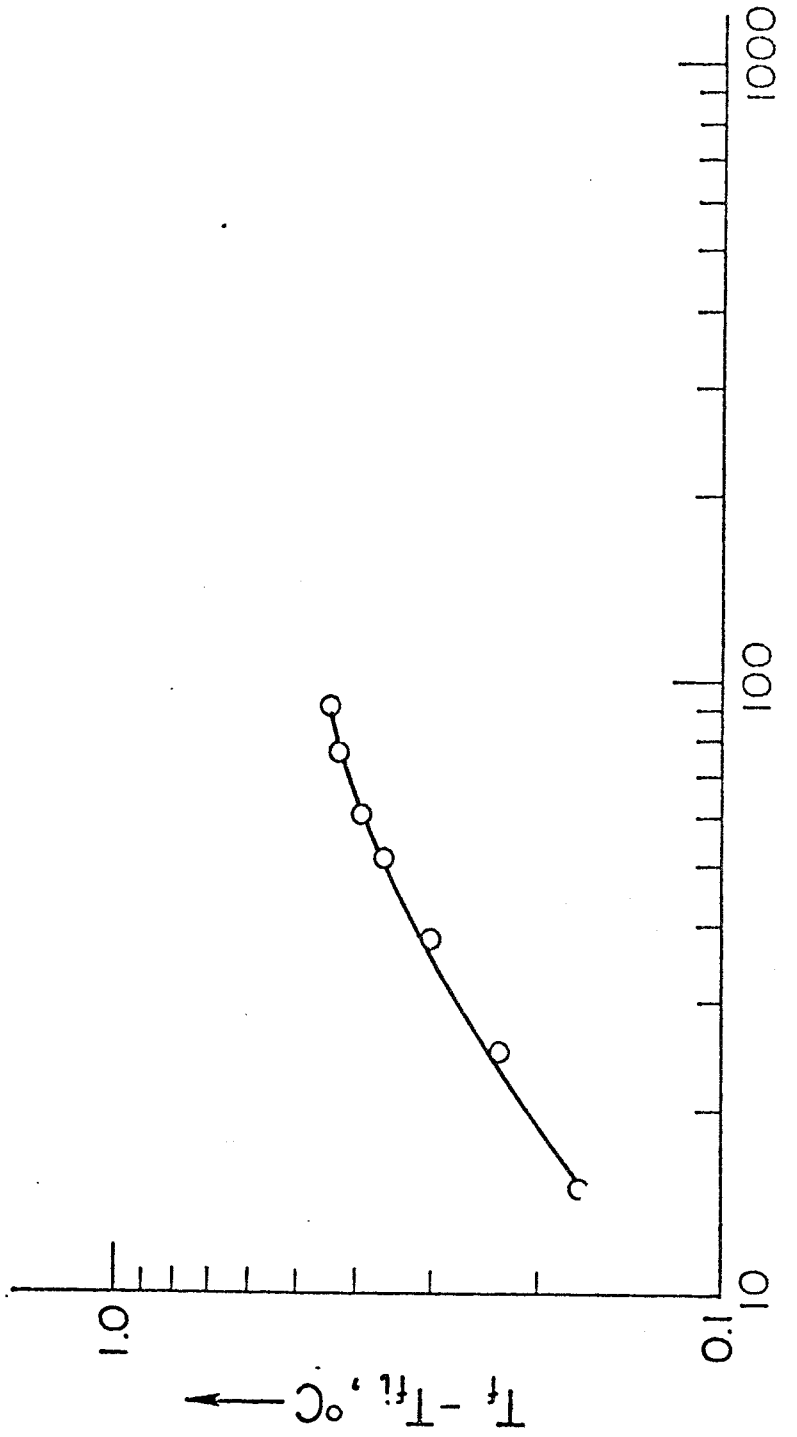

Figure 17. Heat Transfer from a Porous Sphere to the Surrounding Fluid

mass transfer process can be represented by a mathematical model similar to equation (26):

$$\frac{\partial C}{\partial \theta} = D_e \frac{1}{r^2} \frac{\partial}{\partial r}\left(r^2 \frac{\partial C}{\partial r}\right) \qquad (26)$$

where C = concentration of tritiated water

D_e = intrasphere effective diffusivity of tritiated water

It is assumed that no transport resistance exists at the interface when intrasphere transport is considered. Equations (25) and (26) can be written in dimensionless variables as:

$$\frac{\partial T}{\partial \theta_h^*} = \frac{1}{r^{*2}} \frac{\partial}{\partial r^*}\left(r^{*2} \frac{\partial T^*}{\partial r^*}\right) \qquad (27)$$

$$\frac{\partial C^*}{\partial \theta_m^*} = \frac{1}{r^{*2}} \frac{\partial}{\partial r^*}\left(r^{*2} \frac{\partial C^*}{\partial r^*}\right) \qquad (28)$$

where $T^* = \dfrac{T - T_{wi}}{T_{si} - T_{wi}}$

$$C^* = \frac{C - C_{wi}}{C_{si} - C_{wi}}$$

$$\theta_h^* = \frac{\alpha \theta}{r^2}, \text{ Fourier Number}$$

$$\theta_m^* = \frac{D_e \theta}{R^2}$$

$$r^* = \frac{r}{R}$$

R = radius of the porous sphere

Equations (27) and (28) have the same solution. Thus, the dimensionless times, θ_h^* and θ_m^*, should be the same for reaching the following conditions:

$$(T - T_{wi}) = 0.1\ (T_{si} - T_{wi}), \text{ and}$$

$$(C - C_{wi}) = 0.1\ (C_{si} - C_{wi})$$

The effective thermal diffusivity can be approximated as 8.75×10^{-3} cm^2/sec. The effective mass diffusivity of tritiated water is about 9.37×10^{-5} cm^2/sec from preliminary experimental data. Therefore, the ratio of real times required for reaching $(T - T_{wi}) = 0.1\ (T_{si} - T_{wi})$ and $(C - C_{wi}) = 0.1\ (C_{si} - C_{wi})$ is:

$$\frac{\theta_h}{\theta_m} = \frac{10^{-5}}{8.75 \times 10^{-3}} = 4.07 \times 10^{-4}$$

From the preliminary experiments, θ_h = 80 sec and θ_m = 5,000 min. Therefore,

$$\left(\frac{\theta_h}{\theta_m}\right)_{experiment} = \frac{80 \text{ sec } (1 \text{ min}/60 \text{ sec})}{5{,}000 \text{ min}} = 2.7 \times 10^{-4}$$

This suggests that heat transfer is accomplished much faster than mass transfer.

INTERFACE TRANSPORT

Forced heat convection from a sphere can be computed from the following relation:

$$\frac{h_t D}{k_f} = 2.0 + 0.6\left(\frac{D v_\infty \rho_f}{\mu_f}\right)^{1/2} \left(\frac{C_\rho \mu}{k}\right)_f^{1/3} \quad \text{.....(29)}$$

where $\frac{h_t D}{k_f}$ = Nu , Nusselt number

$\frac{D v_\infty \rho_f}{\mu_f}$ = Re , Reynolds number

$\frac{C_\rho \mu}{k}$ = Pr , Prandtl number

Equation (29) requires Nu = 2 for a motionless fluid. The subscribe "f" represents the property of a fluid. Similarly, forced mass transfer from a sphere can be estimated from:

$$\frac{h\,D}{\rho_f D} \quad 0 + 0.6\left(\frac{D\nu_\infty \rho_f}{\mu_f}\right)^{1/2}\left(\frac{\mu}{\rho D_e}\right)^{1/3} \qquad (30)$$

where $\frac{h_m D}{\rho_f D_e}$ = Sh , Sherwood number

$\frac{\mu}{\rho D_e}$ = Sc , Schmidt number

This equation also predicts Sh = 2.0 for a motionless fluid.

The limiting case when the fluid is motionless may be used to compare the relative importance of mass and heat transfer for interface energy transfer at low Reynolds numbers. For this case, we can obtain the following relation from equations (29) and (30).

$$Nu = Sh = 2.0$$

or $$\frac{h_t D}{k_f} = \frac{h_m D}{\rho_f D_e} = 2.0$$

The numerical values used for the physical constants are as follows:

$D = 2$ in = 5.08 cm

$k_f = 0.343$ BTU/hr-ft-^oF

$\rho_f = 1$ gm/cc

$D_e = 10^{-5}$ cm^2/sec

Therefore, both heat and mass transfer coefficients can be estimated as follows:

$$h_t = \frac{2.0 k_f}{D} = \frac{2.0 \text{ X } 0.343 \text{ BTU/hr-ft-F}}{2 \text{ X } 1/12 \text{ ft}} = 4.12 \text{ BTU/hr-ft}^2\text{-}^oF$$

$$h_m = \frac{2.0\ \rho_f\ D_e}{D} = \frac{2.0 \text{ x } 1 \text{ g/cm}^3 \text{ x } 10^{-5} \text{ cm}^2\text{/sec}}{5.08 \text{ cm}^2} = 3.79 \text{ x } 10^{-6} \frac{g}{cm^2\text{-sec}}$$

$$= 2.79 \text{ X } 10^{-2} \frac{lb}{ft^2\text{-hr}}$$

The energy transport due to heat transfer, q_t, can be written as:

$$q_t = h_t \text{ A } \Delta T \quad \ldots\ldots\ldots\ldots\ldots\ldots\ldots\ldots\ldots\ldots\ldots\ldots\ldots\ldots\ldots\ldots\ldots\ldots \qquad (31)$$

The energy transport due to mass transfer, q_m, can be written as:

$$q_m = h_m \, A \, \Delta T \, C_p \quad \text{.....(32)}$$

The ratio of energy transfer due to these two different mechanisms can be obtained from equations (31) and (32) as:

$$\frac{q_t}{q_m} = \frac{h_t}{h_m C_p} = \frac{4.12}{2.79 \times 10^{-2} \times 1.0} = 148 \quad \text{.....(33)}$$

From equation (33), the energy transfer at the interface in the low Reynolds number region is mainly a result of heat transfer. The mass transfer mechanism can be neglected.

In the second case, when the flow regime is in a high Reynolds number region, the last terms on the right-hand side of equations (29) and (30) are much larger than 2.0. Therefore, the following approximations hold:

$$Nu \doteq 0.6 \, (Re)^{\frac{1}{2}} \, (Pr)^{\frac{1}{3}}$$

$$Sh \doteq 0.6 \, (Re)^{\frac{1}{2}} \, (Sc)^{\frac{1}{3}}$$

or:

$$\frac{Nu}{Sh} \doteq \frac{(Pr)^{\frac{1}{3}}}{(Sc)^{\frac{1}{3}}} \quad \text{.....(34)}$$

The numerical values for Pr and Sc of water can be calculated as:

$$Pr = \frac{C_p \mu}{k} = \frac{1 \text{ Btu/lbF} \times 2.42 \text{ lb/ft hr}}{0.343 \text{ Btu/hr ft F}} = 7.06 \quad \text{.....(35)}$$

$$Sc = \frac{\mu}{\rho D_e} = \frac{10^{-2} \text{ g/cm sec}}{\left(1 \text{ g/cm}^3\right)\left(10^{-5} \text{ cm}^2/\text{sec}\right)} = 10^3 \quad \text{.....(36)}$$

Substituting equations (35) and (36) into equation (34), yields:

$$\frac{Nu}{Sh} = \left(\frac{7.06}{10^3}\right)^{\frac{1}{3}} = 0.192$$

or:

$$\frac{\frac{h_t D}{k}}{\frac{h_m D}{\rho D_e}} = 0.192 \quad \text{.....(37)}$$

Rearranging equation (37) yields:

$$\frac{h_t}{h_m} = \frac{0.192\ k}{\rho\ D_e}$$

The ratio of energy transfer due to heat and mass transfer can be estimated as:

$$\frac{q_t}{q_m} = \frac{h_t}{h_m c_p} = \frac{0.192\ k}{\rho\ D_e\ C_p} =$$

$$= \frac{(0.192)\ (0.343)\ \text{Btu/hr-ft-F}}{1\ \text{g/cm}^3 \times 10^{-5}\ \text{cm}^2/\text{sec} \times 1\ \text{Btu/lb F} \times 3600\ \text{sec/hr} \times \text{lb}/450\text{g} \times 12\text{cm/ft}}$$

$$= 65.9 \quad \text{.....(38)}$$

Equation (38) suggests that energy transfer at the interface is mainly a result of heat transport, rather than mass transport.

MATHEMATICAL MODELLING

Work done on the mathematical modelling of two-phase flow since June, 1974 has taken two main directions. The first of these is a study and evaluation of the fundamental characteristics of nonisothermal two-phase boiling flow in porous media. Specifically this involves an examination of the validity of the Darcy law for multi-phase flow under nonisothermal conditions. It also has the purpose of developing a theoretical foundation for the laboratory determination of the appropriate form of the nonisothermal flow rate equation. The second direction has been to develop plans for the refinement and generalization of the numerical simulation computer program described in Progress Report No. 3 (Kruger and Ramey, 1974).

FLJNDAMENTAL CHARACTERISTICS OF NONISOTHEEMAL FLOW IN POROUS MEDIA

One traditional approach to describing nonisothermal flow processes in porous media has been to use concepts from the isothermal flow situation and to extend them to the more complicated nonisothermal situation. Thus, the Darcy law for single- and multi-phase flow is combined with equations of state and a statement of mass conservation. As a consequence of the nonuniform temperature field, an equation describing conservation of energy must also be prescribed. The possibility of a temperature effect on the Darcy law seems to have been widely neglected (e.g., Miller, 1951; Landrum et al, 1960; Wilman et al, 1961; Lasseter and Witherspoon, 1974). Recent experimental work on the effect of temperature on both single- and two-phase flow in porous media suggests that such effects may be too great to be neglected. These results have been reviewed by Ramey et al (1974, page 17), although this review does not include the results of Cassé (1975).

Thus, there is a need for a fundamental examination of the nature of nonisothermal fluid flow in porous media. The proposed work described in this section will have the purpose of laying the theoretical groundwork of what ultimately must be an experimental verification of some form of transport law for nonisothermal fluid flow in a porous medium. Hence, it will undoubtedly lead to experimental work which will complement the other experiments being carried out in this research project.

The approach to this problem that will be used will be to hypothesize a form of the Darcy law as being valid for nonisothermal flow, for example:

$$v_i = \frac{-k_i(S_i,\ T,\ \text{wetting history})}{\mu_i} \left(\frac{\partial p_i}{\partial s} - \rho_i g \frac{dh}{ds}\right)$$

where v_i is the macroscopic velocity of the ith fluid in the s-direction,

k_i is the effective permeability to the ith fluid (for an isotropic medium),

μ_i is the viscosity of the ith fluid,

S_i is the volumetric fluid saturation of the ith fluid,

T is the local temperature of the medium when viewed as a continuum,

p_i is the pressure of the ith fluid,

s is a direction vector along an arbitrary curve,

ρ_i is the density of the ith fluid,

g is the acceleration due to gravity,

and h is the vertical height above some datum.

For single-phase flow, i would be 1 only, and the permeability, k_i, would be a function of temperature only. This relation has been found to be valid to a good approximation for isothermal flow within certain limits on the flowing conditions (Scheidegger, 1960). The logical extension of Darcy's law to nonisothermal flow discussed here implicitly assumes that

the pressure and gravitational potentials are the only ones causing fluid motion in the porous medium. However, it is known, for example, that mass transport will occur in porous media at low liquid saturations in response to a temperature gradient. This is called thermo-osmosis by Collins (1961, page 58), and is apparently not fully understood. Thus it can be seen that even the above hypothesized form of a Darcy law for nonisothermal flow is known to be incorrect under certain conditions, and that under such conditions an alternate form of transport law must be developed.

Two main approaches will be used in the proposed study. The first will be a fundamental examination of the rate equation itself. The second approach will be to develop analytic solutions to relatively simple flow systems. These results will be developed in order to apply them to experimental work so as to determine the appropriate form of the rate equation. Ultimate emphasis will be on two-phase flow, although non-isothermal single-phase flow will be considered initially as a simplifying case.

There are two general theoretical approaches available for examining the form of the rate equation. In general a rate equation is a macroscopic description of physical phenomena occurring on a microscopic scale. The first theoretical approach could be the macroscopic view of irreversible thermodynamics. This could be used as a basis for hypothesizing the form and content of the rate equation for nonisothermal flow in porous media, The theory for this approach has recently been reviewed by Luikov (1966, pages 13-23), and Bear (1972, pages 85-90). The second theoretical approach available for studying the form of the rate equations is what can be called the microscopic approach. Equations describing the small scale physical phenomena are developed then averaged

in space to represent a continuum description. For example, the form of Darcy's law for single-phase isothermal flow can be deduced from a microscopic consideration of mass, momentum, and energy conservation (Muskat, 1937; Hubbert, 1940; Bear, 1972).

Although these methodologies are useful for suggesting the form that the rate equations might take, they must ultimately be verified in the laboratory. The phenomenological coefficients in these rate equations must always be determined experimentally. Unfortunately such experimental determination of flow coefficients can be fraught with difficulties. For example, the measurement of bulk fluid saturation in multi-phase flow experiments mustusuallybe done indirectly, and methods which are used for isothermal flow become difficult to apply under conditions of nonisothermal boiling flow. The capacitance saturation probe described elsewhere in this report is being developed with the purpose of overcoming some of these difficulties.

On the basis of theory describing isothermal two-phase flow it should be possible to develop analytic methods for determining the form of nonisothermal rate equations directly from simple experimental results. This basis is the frontal advance theory proposed by Buckley and Leverett (1942), and later extended to dynamic displacement determinations of relative permeability by Welge (1952), and Johnson et.al. (1959). Such dynamic displacement determinations require the measurement of fluid in- and out-flows, and the pressure drop across the system as functions of time. They do not require in-place measurement of volumetric liquid saturation, and hence can be convenient to run.

Under certain conditions it is possible to describe single-phase nonisothermal flow in porous media in a manner directly analagous

to the theory of Buckley and Leverett. Furthermore, the analogy can be continued and also applied to single-phase dynamic displacement experiments of hot or cold fluid injection. Under limiting conditions the temperature effect on single-phase permeability can actually be determined by a dynamic experiment analogous to that of Johnson et al. Under more general conditions numerical techniques (Squire, 1970) are available for determining the single-phase permeability as a function of temperature. In each case the dynamic displacement procedure requires the measurement of only in- and out-flows, and total pressure drop across the system. These procedures produce results characteristic of nonisothermal flow. This is in contrast to the fact that up until now all measurements of the effect of temperature on permeability have been under isothermal flowing conditions only.

Even though the evaluation of nonisothermal single-phase permeability can be accomplished with more simple analysis than that required for the above described procedures (by additionally measuring pressure and temperature profiles), there is good reason for developing this dynamic displacement theory further. Methods for in-situ field measurement of single-phase permeability under nonisothermal flowing conditions could be developed using it. The possibility for extending such methods to two-phase boiling flow also exists. This could reduce (but not eliminate) the present need for measuring pressure and volumetric liquid saturation profiles along laboratory cores.

NUMERI SI AT

A numerical simulation program was developed for performance matching of the bench-scale experiments immediately, and for extension to field performance forecasting eventually. Some of the features and results of this program were presented in Progress Report No. 3 (Kruger and Ramey, 1974). A project report on this computer model is being prepared and will be issued in the next quarter. This report will include the program, documentation, and other example applications than presented previously. In keeping with RANN objectives, the program has already been made available to personnel of other geothermal research projects on request.

Although the model has been used successfully to match experiments of Arihara (1974), and to obtain a better understanding of the dynamic behavior of the experimental geothermal model studies by Cady (1972), there are several drawbacks to operation of the program in its present form.

One of the drawbacks of the present computer model is that it is sometimes awkward to apply to realistic physical situations. This is due to the limitations that only boiling two-phase linear flow can be described, and that it can handle only a specific set of boundary conditions. Thus, neither the development of a two-phase flow region beginning from the single-phase compressed liquid state can be described, nor can the development of a single-phase superheated steam zone beginning from the two-phase boiling state be described. Both of these transitions are of considerable practical interest. Since both of these problems involve a moving boundary, the problem of obtaining a numerical solution is somewhat increased. However, approximate finite difference methods such as those reported by Coats et al (1974) and Weinstein et al (1974) could be used.

The model could easily be extended to the radial flow geometry describing the flow to a single well in the absence of vertical segregation

Squire, W., Integration for Engineers and Scientists, American Elsevier, 1970.

Stoker, A. K., and Kruger, P., Radon Measurements in Geothermal Systems, SGP-TR-4, NSF Grant No. GI-34925, Stanford University, January, 1975.

Strobel, C.J., "Model Studies of Geothermal Fluids Production from Consolidated Porous Media," Engineer's Thesis, Stanford University, July, 1973.

Thomas, A.M., "In Situ Measurement of Moisture in Soil and Similar Substance by 'Fringe' Capacitance," Sci. Instrum., 1966, Vol. 43, 21-27.

Todd, M.R., O'Dell, P.M., and Hirasaki, G.J., "Methods for Increased Accuracy in Numerical Reservoir Simulators," Trans. AIME, 253 (1972), 515-30.

Warren, W.J., "BS & W Measurement--Principles and Practices," J. Pet. Tech., November, 1962, 1207-12.

Weinstein, H.G., to Atkinson, P.G., Personal Communication, October 3, 1974.

Weinstein, H.G., Wheeler, J.A., and Woods, E.G., "Numerical Model for Steam Stimulation," SPE 4759, presented at Improved Oil Recovery Symposium of SPE, Tulsa, Oklahoma, April 22-24, 1974.

Welge, H.J., "A Simplified Method for Computing Oil Recovery by Gas or Water Drive," Trans. AIME, 195 (1952), 91.

Willman, B.T., et al., "Laboratory Studies of Oil Recovery by Steam Injection," Trans.AIME, 222 (1961), 681.

STANFORD GEOTHERMAL PROJECT REPORTS

SGP-TR-1 Kruger, Paul, and Ramey, Henry J., Jr., Stimulation and Reservoir Engineering of Geothermal Resources, Progress Report No. 3, June, 1974.

SGP-TR-2 Arihara, Norio, A Study of Non-isothermal and Two-phase Flow Through Consolidated Sandstones, November, 1974.

SGP-TR-3 Casse, Francis J., The Effect of Temperature and Confining Pressure on Fluid Flow Properties of Consolidated Rocks, November, 1974.

SGP-TR-4 Stoker, Alan K., and Kruger, Paul, Radon Measurements in Geothermal Systems, January, 1975.

SGP-TR-5 Kruger, Paul, and Ramey, Henry J., Jr., Stimulation of Geothermal Aquifers, Progress Report No. 1, March, 1973.

SGP-TR-6 Ramey, H.J., Jr., Brigham, W.E., Chen, H.K., Atkinson, P.G., and Arihara, N., Thermodynamic and Hydrodynamic Properties of Hydrothermal Systems, April 20, 1974.

SGP-TR-7 Hunsbedt, Anstein, Kruger, Paul, and London, Alexander L., A Laboratory Model of Stimulated Geothermal Reservoirs, February, 1975.

ACKNOWLEDGEMENT

This work was supported by the National Science Foundation. In keeping with the objectives of the RANN program, communications were maintained with many academic, industrial, and government agencies. Acknowledgement *is* made for the advice and cooperation given us by these several agencies.